Eddy dynamics of β plumes

by

Shinichiro Kida

B.Sc. in Earth and Planetary Physics
The University of Tokyo, 2000

Submitted in partial fulfillment of the requirements for the degree of

Master of Science

at the

MASSACHUSETTS INSTITUTE OF TECHNOLOGY

and the

WOODS HOLE OCEANOGRAPHIC INSTITUTION

September 2003

Author .....
Joint Program in Oceanography/Applied Ocean Science and Engineering
Massachusetts Institute of Technology
Woods Hole Oceanographic Institution
September, 2003

Certified by .....
Jiayan Yang
Associate Scientist
Thesis Supervisor

Certified by .....
James F. Price
Senior Scientist
Thesis Supervisor

Accepted by .....
Carl Wunsch
Chairman, Joint Committee for Physical Oceanography
Massachusetts Institute of Technology
Woods Hole Oceanographic Institution

Eddy dynamics of β plumes

by

Shinichiro Kida

Submitted to the Massachusetts Institute of Technology
and the Woods Hole Oceanographic Institution
in partial fulfillment of the requirements for the degree of
Master of Science

Abstract

The importance of eddies and nonlinearities in β-plume dynamics in the deep ocean was investigated using reduced gravity models of the deep ocean forced by a small region of cross isopycnal transport in the interior. The effect of topography on β-plumes was also examined by placing a Gaussian bump in the forcing region. Despite the fact that the mean flow is weak in the deep ocean interior, it was found that the nonlinearity and instabilities are still important for realistic parameter and forcing values. The flow was dominated by eddies and was remarkably different from what would be expected from a linear solution.

Thesis Supervisor: Jiayan Yang
Title: Associate Scientist

Thesis Supervisor: James F. Price
Title: Senior Scientist

Acknowledgments

I would like to thank my advisers, Dr. Jiayan Yang and Dr. Jim Price for spending enormous amount of time for discussion and guidance. I can not thank them enough for the advice and feedback they provided me. In addition to the weekly discussions, their constant warm support made it possible for me to enjoy my research and also the field of Physical Oceanography. I would also like to thank Dr. Karl Helfrich for guiding me through much of the literature on hydrothermal plumes. The research on this topic would not have gone as smoothly without his help. My thanks also goes to Dr. Joe Pedlosky for thorough answers to many of my questions, Prof. John Marshall for the providing me the computer resources at MIT, and my thesis committee members, Drs. Robert Beardseley, Glenn Flierl, and Carl Wunsch for their valuable comments that improved many parts of this study.

I feel very fortunate to have such wonderful classmates, J. Tom Farrar, Jason Hyatt and Mitch Ohiwa. Their encouragement through the years meant a lot to me. The discussions with Geoffrey Gebbie, Baylor Fox-Kemper, and Taka Ito also improved my research. Thanks also to my officemates, Juan Botella, Juli Atherton, Fabio Dalan, David Stuebe, and Max Nikourachine for making my life at MIT comfortable.

Last, I would like to thank my parents, Hideji and Yasuko Kida. Their love and support from Japan made it possible for me to enjoy my studies here in the United States.

This study was supported by Woods Hole Oceanographic Institution Academic Programs Office Fellowship and National Science Foundation Grant 89542700.

Contents

Chapter 1

Introduction

1.1 What is a β-plume?

A β-plume is a large scale horizontal circulation driven by a localized mass source or sink. It was introduced by Stommel (*Stommel 1982*) who was inspired by an observational result which show an anomaly of helium from the hydrothermal vents extending to the west of East Pacific Rise (*Lupton 1984*). This feature was unexpected at the time, for the circulation at this location ($90^o - 134^oW, 15^oS$) was believed to be a weak southeast flow according to the Stommel and Arons Model (*Stommel and Arons 1960*). Stommel then showed that a hydrothermal vent is capable of driving a large horizontal circulation on its own by using a linear vorticity balance equation;

$$\beta v = \frac{f_o w^*}{H} \tag{1.1}$$

where f_o, β, v, w^*, and H are the Coriolis parameter, its meridional gradient, meridional velocity, cross isopycnal velocity, and layer thickness respectively. More detailed description of this equation and terms will be given later. This linear vorticity equation (Eq 1.1) is a balance between planetary vorticity advection (LHS) and vortex stretching($w^* > 0$) or squashing($w^* < 0$) (RHS). For a wind driven gyre where this linear vorticity balance is known as Sverdrup balance, Ekman pumping causes vortex stretching/squashing and drives a meridional flow. For a β-plume, the cross isopycnal

transport created by the hydrothermal vents causes vortex stretching/squashing and drives a meridional flow. However, the meridional flow can establish only in limited areas because unlike wind forcing, hydrothermal vents do not exist all over the basin. Figure 1-1 shows the basic concept schematically. Through geothermal heating, the water near the vent is heated and rises to its neutrally buoyant layer as it entrains the surrounding water. For the neutrally buoyant layer, this cross isopycnal transport leads to vortex squashing. From Eq 1.1, vortex squashing creates a southward flow. In order to balance this southward flow, there needs to be a northward flow somewhere in the basin. Since there can not be any meridional flow in the interior where hydrothermal vents do not exist, an anticyclonic circulation consisting of a northward western boundary flow, a westward zonal jet and an eastward zonal will establish. For the layer below the neutrally buoyant level, the opposite mechanism causes vortex stretching and a cyclonic circulation will establish. Figure 1-2 is the steady solution for each layer. A linear two-and-a-half layer reduced gravity model described in the next chapter was used to calculate this steady solution. These two counter rotating circulations are what has been called the "β-plume." The concept of β-plumes provided a mechanism for creating a strong zonal flow in the deep ocean.

A small cross isopycnal transport is capable of forcing a horizontal circulation of much larger order of magnitude than itself. For example, at 30^oN, the linear vorticity balance (Eq 1.1) shows that a cross isopycnal transport of 0.01 Sv over an area 100km(meridional) $\times$ 100km(zonal) is capable of creating a horizontal transport of 3.5 Sv. The ratio of total cross isopycnal transport(W) to horizontal transport(M) depends on a parameter $f/\beta L$ which is a function of the latitude and meridional length scale L of where the cross isopycnal transport exists. [*Pedlosky 1996, Spall 2000*]. Suppose a region of constant cross isopycnal velocity (forcing region) exists in the interior as shown in Figure 1-3a. From linear vorticity balance, the total meridional transport(M) across this forcing region is,

$$M = vHL_x = \frac{fw^*}{\beta}L_x \tag{1.2}$$

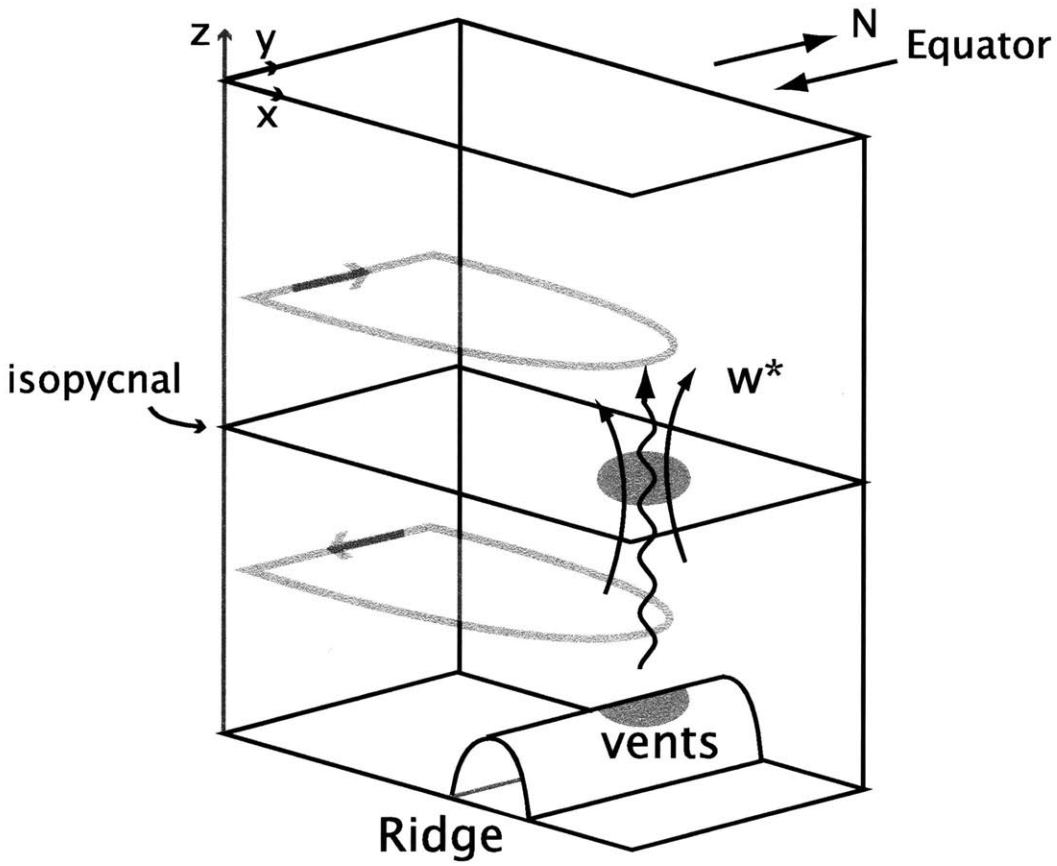

Figure 1-1: Schematic Picture of a β-plume adapted from *Stommel(1982)*. The upper layer represents the neutrally buoyant density layer and the bottom layer represents the layer below. The left boundary represents the western boundary. The water heated by the vent entrains the surrounding water from the bottom layer and enters the upper layer with a total cross isopycnal transport of W^*. As a result of this cross isopycnal transport, a cyclonic circulation is established in the bottom layer and an anticyclonic circulation is established in the upper layer.

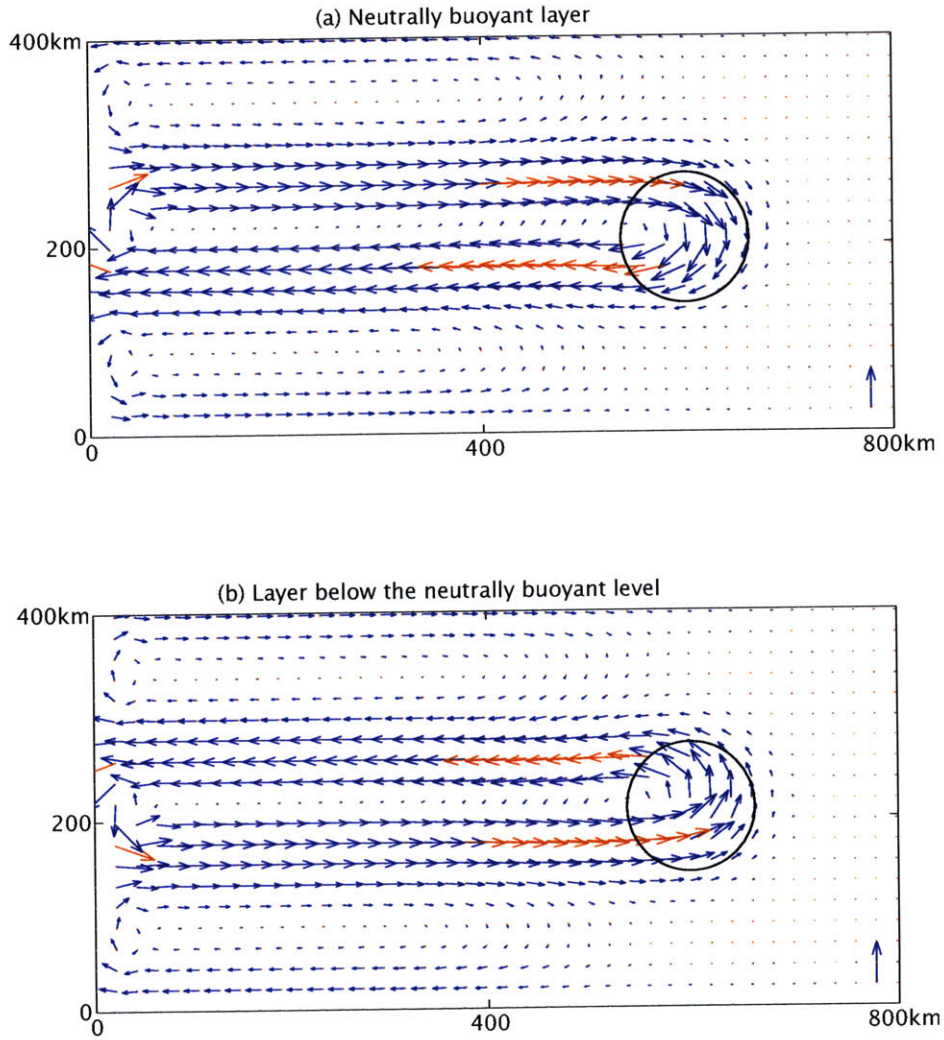

Figure 1-2: Velocity field in the (a) Neutrally buoyant layer and (b) Layer below are shown. The black circles indicates the forcing region. Velocity larger than 0.01 m/s are truncated and are shown in red. Only the values at every 5 grid points are shown. For scaling, 0.01 m/s is shown in the bottom right corner
(a) shows an anticyclonic circulation and (b) shows a cyclonic circulation. Meridional flow exists only in the forcing region and the western boundary connected by the two zonal jets. The weak zonal jets at the southern and northern boundary (in both figures) are created by the weak uniform background flow from the upper layer to the layer below. It is a weak Stommel and Arons type of circulation and thus is not strongly interacting with the β-plume circulation.

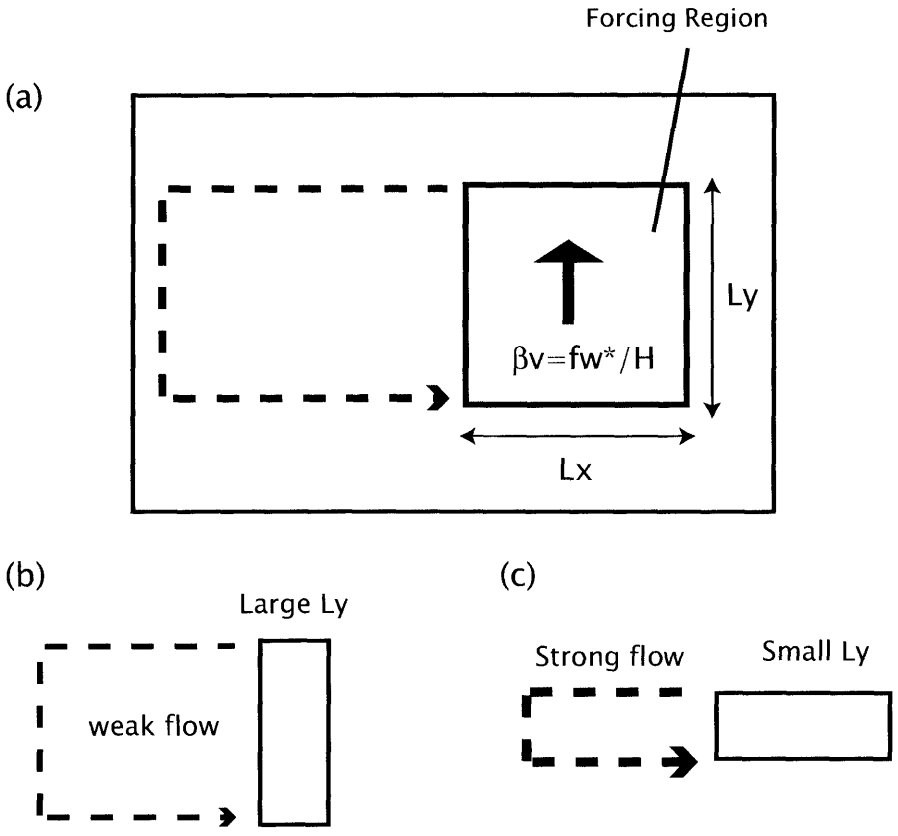

Figure 1-3: A schematic of a β-plume when the water mass is leaving the layer: (a) The region of intense cross isopycnal velocity (forcing region) is located in the interior of a rectangular basin. Assuming that the linear vorticity balance holds inside this forcing region, the total horizontal transport induced by the forcing is $M = vL_x = \frac{fw^*}{\beta H} L_x$. Using the total cross isopycnal transport ($W = w^* L_x L_y$) across the forcing region, $\frac{M}{W} = \frac{f}{\beta L_y H}$. The ratio shows that the induced horizontal transport is inversely proportional to L_y as shown schematically in (b) and (c).

The total cross isopycnal transport in the forcing region is $W = w^* L_x L_y$ so this equation (Eq 1.2) becomes

$$\frac{M}{W} = \frac{f}{\beta L_y H}. \tag{1.3}$$

This parameter shows that the total meridional transport is inversely proportional to the meridional length scale of the forcing region.

Studies on β-plumes progressed by solving the steady problem through theory, primarily because only a few observations were available in the deep ocean. It might be argued that β-plumes are localized processes and thus might be insignificant in the presence of mean flows such as those in the Stommel and Arons model, topographic effects , and wind forcing. Prior effort focused on this problem finds the β-plume still significant enough in some region to compete with the mean flow and to drive the deep circulation. *Speer (1989)* showed that the existence of a β-plume in the presence of a background Stommel and Arons flow depends on the ratio of long wave speed to the background flow which is large enough to overcome the background flow in some places. *Hautala and Riser (1993b)* investigated a β-plume in the presence of background Stommel and Arons flow, topography, and wind forcing by solving a steady geostrophic three layer model. Their result also showed the strength of the β-plume to be significant enough to compete with other effects, at least locally. An observational work of *Hautala and Riser (1993a)* which showed the effect of β plumes in the deep ocean, also seems to be in support of the previous theoretical studies.

The concept of β-plumes have been applied to regions besides deep ocean such as the Mediterranean overflow. Localized entrainment of Atlantic Ocean water into the overflow water is driving the β-plume in this case. Since w^* is negative, the mechanism for this β-plume works in the opposite sense creating a cyclonic gyre in the upper layer and an anticyclonic gyre in the lower layer since w^* is negative. *Jia (2000)* showed this mechanism to be a possible cause for the Azores current. *Spall (2001)* and *Özgökmen and Crisciani (2000)* showed that friction is capable of diminishing or completely wiping out the β-plume when the forcing region (mass sink/source) is along the eastern boundary. The role of friction can not be neglected in β-plume

dynamics if the mass sink/source is close to the boundary.

There have been only a few studies on the effect of nonlinearities and instabilities on β-plumes. The results of *Özgökmen et al. (2001)* shows the presence of barotropic instabilities in their calculations of the Mediterranean overflow case, although no detailed analysis of the role of these instabilities were given. β-plumes are also two layer events and baroclinicity can become important. How β-plumes are affected by nonlinearities and instabilities is an open question and will be a focus of this study.

1.2 Single Hydrothermal Plume Events

Single hydrothermal plume events have been studied theoretically (*Speer 1989*), numerically (*Speer and Marshall 1995*), and through laboratory experiments [e.g. *Helfrich and Battisti (1991)*]. Most work concentrated on the formation and breaking mechanisms of a single plume event. A hydrothermal plume first rises to a level of neutral buoyancy and then starts to spread out laterally, forming a lenselike structure. This lenselike structure creates an anticyclonic vortex in the neutrally buoyant density layer and a cyclonic vortex below this layer. The lens structure is maintained as the plume increases laterally until it reaches the size of the deformation radius. Then, the lens structure begins to break apart. The anticyclonic vortex in the neutrally buoyant layer splits into an anticyclonic vortex and a cyclonic vortex and many vortices of different sign will eventually emerge in the region with each vortex having no particular preference on the direction in which it propagates (*Hogg and Stommel 1985*).

The evolution of a single plume in the deep ocean is difficult to observe. *Joyce et al. (1998)* showed two vortices of different sign on top of each other formed in one of the mega plume events in its early stages. *D'Asaro et al. (1994)* also found a vortex structure both in the young and mature mega plumes. Observations seem to support the formation mechanism outlined above.

The studies of a single plume event have been mainly based on a f-plane. This is because each plume event occurs on the order of a few kilometers and the change in

f is negligible. The nonlinear nature of two vortices of different sign on top of each other have been well studied (e.g. *Flierl (1988)*) on the f-plane, but if a large scale effect of hydrothermal plumes were to be considered, β cannot be neglected from its dynamics. Nonlinear behavior of the large scale plume will be influenced by β which could stabilize the vortex breaking observed in a f plane model. While there have been many studies on nonlinear behavior of individual plume events in small scales, the nonlinear behavior of the large scale mean of many single plumes has not been well studied.

1.3 Topography

Hydrothermal vents typically lie on mid ocean ridges where topographic variations are large compared to other parts of the ocean interior. Overflows also exist where topographic variations are large. The regions where the concept of β-plumes are applied coincide to regions where topographic variation is considered large. The importance of topography on β-plumes has been addressed in some previous studies (*Speer 1989*), although its actual effect has not been studied adequately. The topographic variations can modify the background Potential Vorticity (PV) gradient, which will likely change the basic circulation.

Kawase and Straub (1991) and *Straub and Rhines (1990)* investigated the effect of topographic variation on the Stommel and Arons Flow. Although their studies are based on the Stommel and Arons flow, they showed an establishment of two zonal jets to the west of the topography similar to β-plumes. This occurred when the topographic variation was large enough to create a region of closed PV contour. These two zonal jets existed roughly along the same latitude and were flowing in the opposite direction. Uniform mixing across the basin is capable of creating zonal jets in the presence of topography. However, further investigation is needed for cases when mixing is localized instead of uniform across the basin. The topographic effect of nonlinearity and instability will also need further investigation.

1.4 Present work

The motivation of this work is to examine the role of eddies and nonlinearities on the dynamics of β-plumes. As mentioned in the previous sections, past studies of large scale β-plumes have focused more on linear dynamics while eddies were usually neglected. However, this does not necessarily mean that the large scale plume has to be governed by linear dynamics. For example, can the narrow zonal jets really exist? Are they stable? Nonlinearities and instabilities could play an important role and influence the β-plume.

Past studies of single hydrothermal plume events have focused on the formation and breaking mechanism on a f-plane. The behavior of a large scale plume, representing series of single hydrothermal events with a large scale mean, will likely be influenced by β and behave differently from a single plume event. However, the nonlinear dynamics of single plume events turned out to be quite relevant to β-plumes found in this thesis. This thesis attempts to show that eddies and nonlinearities do influence the large scale β-plume with its dynamics somewhat similar to the f plane dynamics. It should be noted that the eddies that will be shown in this study are not the hydrothermal eddies created by some particular hydrothermal plume event or from interaction between hydrothermal plumes. A large scale mean of the effect of many hydrothermal events was used because the resolution was not high enough to sufficiently resolve the dynamics of each hydrothermal plume event.

Topographic effects will also be investigated. Not only can topography change the structure of the β-plume but it can also change the instability mechanism because of the topographic β effect. The importance of nonlinearities and instabilities can also change with the topographic variation.

Figure 1-4 is a result of the same reduced gravity model as the one used for Figure 1-2 but now with nonlinearity and varied bottom topography. Compared to Figure 1-2 where the model was linear with a flat bottom, it is apparent that nonlinearity and varied topography do affect the β-plume. The flow structure is now complicated and its dynamics are not easy to understand. How this complicated flow field was

created will be described in the following chapters by separating the problem into two parts so that it easier to understand. (1) How baroclinicity effects β-plumes. (2) How bottom topography effects β-plumes. The details of the numerical model used in this study are described in Chapter 2. Scaling arguments, PV balance equation and thickness balance equation which will be used when diagnosing the result will also be explained here. The effect of baroclinicity on β-plume with a flat bottom will be described in chapter 3. The effect of topography on the β-plume will be described in chapter 4. Chapter 5 is the summary and conclusion.

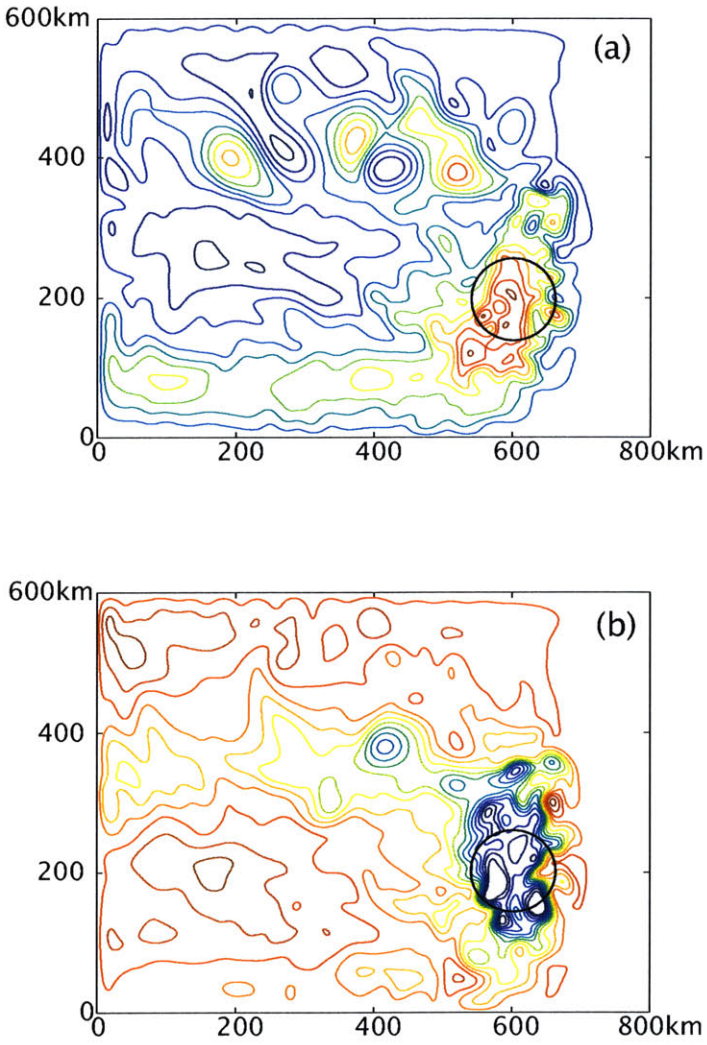

Figure 1-4: An instantaneous pressure field after 100 years of spinup when nonlinearity and bottom topography variation variation are included into the previous two-and-a-half layer linear model (used for Stommel's solution shown in Figure 1-2). The meridional length of the basin is also longer to the north than the previous linear model. The forcing region is indicated by the black circle. High pressure is contoured in red and low pressure is in blue.
The flow in both layers is now dominated by eddies. The large scale anticyclonic and cyclonic circulation expected from the linear dynamics like Figure 1-2 is hard to notice. The flow is roughly geostrophic with the velocities basically along the pressure contours with red to the right. More complete details of this figure will be shown in Chapter 4 where this case will be examined more in detail.

Chapter 2

Model Description and Basic theory

2.1 Numerical Model

A flipped two and a half layer reduced gravity model was used in this study. This model is simple but includes the necessary physics for the purpose of this study. A schematic picture of this model is shown in Figure 2-1. Unlike typical reduced gravity models, the top layer is motionless. There are two moving layers of constant density which represent deep ocean waters. (These two layers represent the neutrally buoyant layer and the layer below which was mentioned in Chapter 1.) The cross isopycnal transport induced by the hydrothermal vents is represented by a prescribed cross isopycnal velocity (w^*) between the two moving layers. The model solves the primitive equations based on the Arakawa C-grid and is based on the model used in *Yang and Price (2000).*

Reduced gravity defined as $g' = \Delta\rho \cdot g/\rho_o$ is set to $5 \times 10^{-4} m/s^2$, where g is the gravitational acceleration and $\Delta\rho$ is the density difference between each layer and the one above. The density difference $\Delta\rho_2$ and $\Delta\rho_3$ where $\Delta\rho_2 = \rho_2 - \rho_1$ and $\Delta\rho_3 = \rho_3 - \rho_2$, are set to be the same. Subscript 1, 2, and 3 represent the top, intermediate, and bottom layer respectively. Initial layer thickness is 500m for both layer 2 and 3. H and g' were estimated from observation of a hydrothermal plume in Juan de Fuca

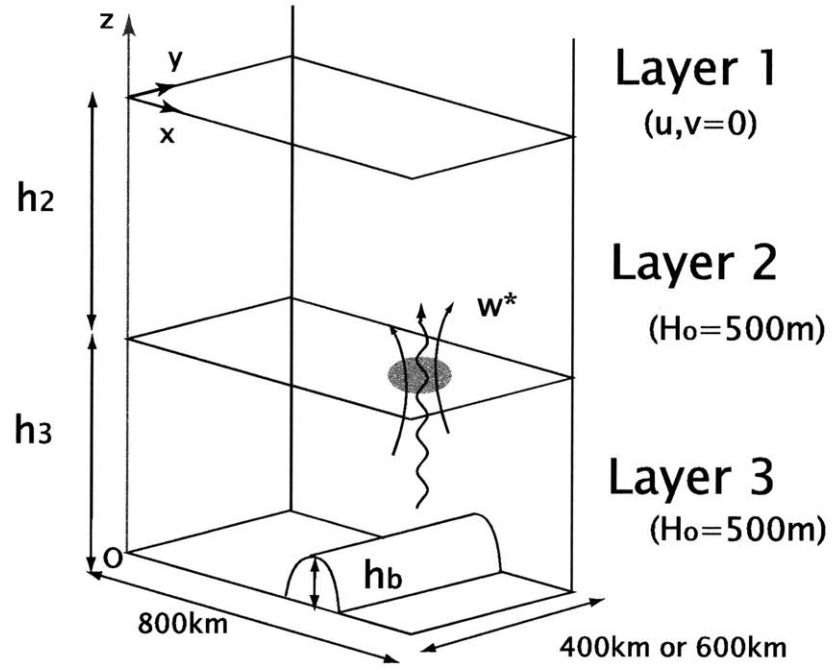

Figure 2-1: Schematic of the Reduced Gravity Model: The top layer(Layer 1) is motionless. x and y axis is to the east and north respectively. z is the vertical axis measured from the bottom (0). Layers 2 and 3 are the two moving layers which represent the deep ocean waters. Both layers have initial layer thickness 500m. The domain size is 400km or 600km meridionally and 800km zonally. Topographic variation only exists for layer 3.

Ridge (*Baker 1987).* The deformation radius is $R_D^{mode1} = \sqrt{g'(h_1+h_2)}/f_o = 10km$ for baroclinic mode 1 and $R_D^{mode2} = \sqrt{g'\frac{h_1 \cdot h_2}{(h_1+h_2)}}/f_o = 7km$ for baroclinic mode 2.

The β plane approximation ($f = f_o + \beta y$) was used for the Coriolis parameter with its center latitude set to $30^o N$. Local Cartesian coordinates were used with x and y positive to the east and north. The horizontal domain is rectangular, 800km wide zonally and 400km or 600km long meridionally depending on the experiment. The β plane approximation is valid for both cases, $\beta L/f_o \ll 1$.

Lateral viscosity was used for friction with $A_H = 5m^2/s$ which gives a Munk boundary layer width of 6km. The model grid is square, $\Delta x = \Delta y = 2km$, and is sufficient to resolve the Munk western boundary layer and the deformation radius of the two modes mentioned earlier. No slip and no normal flow were used for the lateral boundary condition.

For layer 2, the momentum equation and the continuity equation are [*Pedlosky (1996)*]:

$$\frac{du_2}{dt} - fv_2 = -g'\frac{\partial(h_2+h_3+h_b)}{\partial x} + \mathcal{F}_{2x}, \tag{2.1}$$

$$\frac{dv_2}{dt} + fu_2 = -g'\frac{\partial(h_2+h_3+h_b)}{\partial y} + \mathcal{F}_{2y}, \tag{2.2}$$

$$\frac{\partial h_2}{\partial t} + \frac{\partial(u_2h_2)}{\partial x} + \frac{\partial(v_2h_2)}{\partial y} = w^*. \tag{2.3}$$

For layer 3:

$$\frac{du_3}{dt} - fv_3 = -g'h_3\frac{\partial(h_2+2h_3+2h_b)}{\partial x} + \mathcal{F}_{3x}, \tag{2.4}$$

$$\frac{dv_3}{dt} + fu_3 = -g'h_3\frac{\partial(h_2+2h_3+2h_b)}{\partial y} + \mathcal{F}_{3y}, \tag{2.5}$$

$$\frac{\partial h_3}{\partial t} + \frac{\partial(u_3h_3)}{\partial x} + \frac{\partial(v_3h_3)}{\partial y} = -w^*. \tag{2.6}$$

$\vec{u} = (u, v)$, h, h_b, and ∇ are horizontal velocity, layer thickness, bottom topography, and horizontal gradient vector $(\partial/\partial x, \partial/\partial y)$ respectively. Initial layer thickness for

the layers are set to

$$h_2(t=0) = H_o(=500m) \tag{2.7}$$

$$h_3(t=0) = h_o - h_b. \tag{2.8}$$

w^* is the cross isopycnal velocity defined as,

$$w^* = w - \frac{d\eta}{dt} \tag{2.9}$$

where w is the vertical velocity and η is the absolute height of the interface between layers 2 and 3 ($\eta \equiv h_3 + h_b$). This cross isopycnal velocity is the difference between the vertical velocity and the change in the absolute height of the interface. If the interface height does not change with time, cross isopycnal velocity is identical to vertical velocity. Alternatively, cross isopycnal velocity is identical to the change in the interface height if vertical velocity is zero.

$\mathcal{F}$ is a dissipation term which is defined in each layer as,

$$\mathcal{F}_2 = (\mathcal{F}_{2x}, \mathcal{F}_{2y}) = \frac{A_H}{h_2}\nabla \cdot (h_2 \nabla \vec{u}_2) + w^* \frac{\vec{u}_3 - \vec{u}_2}{h_2}\Theta(w^*), \tag{2.10}$$

$$\mathcal{F}_3 = (\mathcal{F}_{3x}, \mathcal{F}_{3y}) = \frac{A_H}{h_3}\nabla \cdot (h_3 \nabla \vec{u}_3) + w^* \frac{\vec{u}_3 - \vec{u}_2}{h_3}\Theta(-w^*), \tag{2.11}$$

where $\Theta(x)$ is the Heaviside step function

$$\Theta(x) = \begin{cases} 1 & \text{if x} \geq 0 \\ 0 & \text{if x} < 0 \end{cases} \tag{2.12}$$

The first term in the dissipation term $\mathcal{F}$ is lateral viscosity and the second term is momentum transfer between the two moving layers.

Forcing: Cross isopycnal velocity

The model was spun up from rest and forced with a prescribed cross isopycnal velocity between layers 2 and 3 shown in Figure 2-2. A region of intensive cross isopycnal

velocity from layer 3 to 2 is located as

$$w^*_{3\to 2} = w_o exp\left[-(\frac{x-x_o}{\delta x})^2 - (\frac{y-y_o}{\delta y})^2\right],$$

with an e-folding scale of 50km for δx and δy. Maximum cross isopycnal velocity is located at (x_o,y_o) which is 600km from the western boundary and 200km from the southern boundary. The term "Forcing region" will correspond to this intense cross isopycnal velocity region within one e-folding scale. The term "Forcing strength" is used to represent the magnitude of w_o, which controls the strength of the prescribed cross isopycnal velocity.

A weak cross isopycnal velocity returning from layer 2 to 3 is also given to conserve mass in each layer,

$$w^*_{2\to 3} = -\frac{w_o}{A}\iint exp\left[-(\frac{x-x_o}{\delta x})^2 - (\frac{y-y_o}{\delta y})^2\right] dA.$$

where A is the total basin area. This cross isopycnal transport from layer 2 to 3 is distributed uniformly across the basin. Thus, the total cross isopycnal velocity at each point is,

$$\begin{aligned} w^* &= w^*_{3\to 2} + w^*_{2\to 3} \\ &= w_o exp\left[-(\frac{x-x_o}{\delta x})^2 - (\frac{y-y_o}{\delta y})^2\right] - \frac{w_o}{A}\iint exp\left[-(\frac{x-x_o}{\delta x})^2 - (\frac{y-y_o}{\delta y})^2\right] dA. \end{aligned} \tag{2.13}$$

Figure 2-2 shows the distribution of this total cross isopycnal velocity when $w_o = 1\times 10^{-6}$ m/s. This amounts to 0.008 Sv of cross isopycnal transport between layer 2 and 3 which is the same order of forcing strength as used in *Stommel (1982)*.

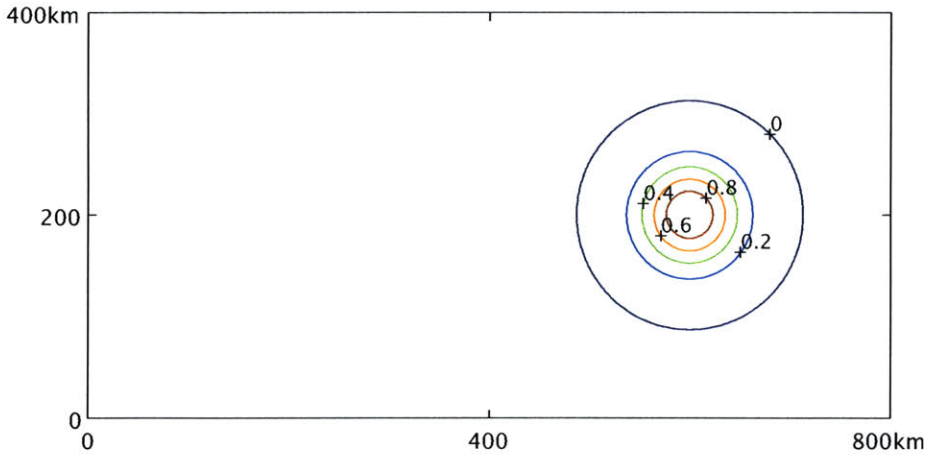

Figure 2-2: Forcing: Cross isopycnal velocity [10^{-6} m/s]. Positive value represents the cross isopycnal transport from layer 3 to 2. Most of the basin has a weak negative value ($\sim -2.5 \times 10^{-8}$ m/s). Maximum cross isopycnal velocity from layer 3 to 2 is located 600km from the western boundary and 200km from the southern boundary, with a value of 1×10^{-6} m/s.

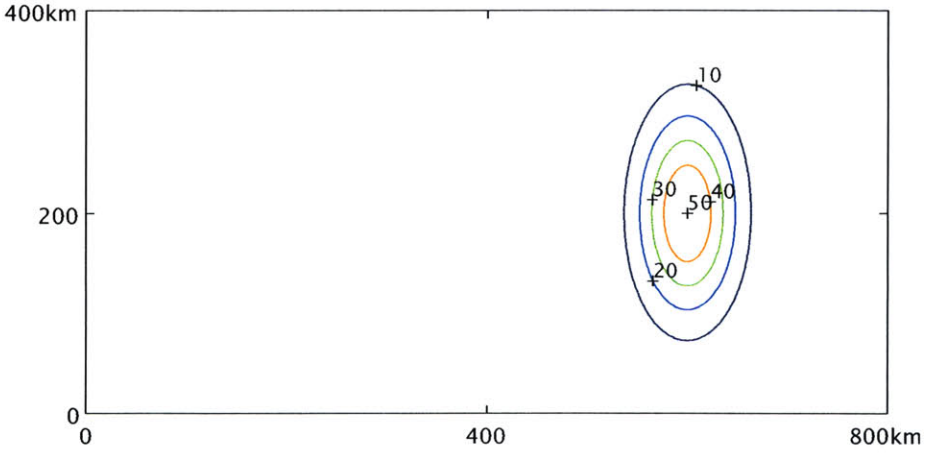

Figure 2-3: Bottom Topography [m]: The maximum height is co-located with the maximum isopycnal transport from layer 3 to 2, i.e., 600km from the western boundary and 200km from the southern boundary. The maximum height is 50 [m] with e-folding length scale 50km zonally and 100km meridionally. The bump is meridionally long and was purposely done so so that the meridional length scale of the forcing and the bump is different.

Topography

For cases with topographic variation, a simple Gaussian bump with e-folding scale of 50km zonally and 100km meridionally shown in Figure 2-3 was used:

$$h_b = h_o exp\left[-(\frac{x-x_o}{l_x})^2 - (\frac{y-y_o}{l_y})^2\right] \tag{2.14}$$

where h_o, l_x and l_y are the maximum height and the e-folding length scale in x and y respectively. The maximum height h_o is 50 m and is located at the same place as the cross isopycnal velocity maximum. Asymmetry was given to this Gaussian bump so that the meridional length scale of the topography and the forcing region is different ($l_y \neq \delta y$). The size of h_o is 10% of the total water column thickness and this magnitude is small compared to the actual values found near the hydrothermal vents.

One-and-a-half layer model

A one-and-a-half layer model was used when the barotropic[1] behavior of a β-plume was examined. Baroclinicity was eliminated by making layer 2 motionless and layer 3 the only moving layer. The momentum equation and continuity equation for layer 3 is, by substituting $\vec{u}_2 = 0$ and $h_2 + h_3 = 0$ into Eq (2.1)-(2.6):

$$\frac{du_3}{dt} - fv_3 = -g'\frac{\partial(h_3+h_b)}{\partial x} + \mathcal{F}_{3x} \tag{2.15}$$

$$\frac{dv_3}{dt} + fu_3 = -g'\frac{\partial(h_3+h_b)}{\partial y} + \mathcal{F}_{3y} \tag{2.16}$$

$$\frac{\partial h_3}{\partial t} + \frac{\partial(u_3h_3)}{\partial x} + \frac{\partial(v_3h_3)}{\partial y} = -w^*, \tag{2.17}$$

[1]The term 'barotropic' is used for the calculations based on the one-and-a-half layer model and 'baroclinic' for the studies based on the two-and-a-half layer model. Although this model is a reduced gravity model and so the one-and-a-half model is technically not a barotropic model but a baroclinic model, these terms are used only to distinguish the two type of models.

where $\vec{\mathcal{F}}_3$ is

$$\vec{\mathcal{F}}_3 = (\mathcal{F}_{3x}, \mathcal{F}_{3y}) = \frac{A_H}{h_3}\nabla \cdot (h_3 \nabla \vec{u}_3) + w^* \frac{\vec{u}_3}{h_3}\Theta(-w^*). \tag{2.18}$$

Linear models

Linear models were used to understand the basic behavior of β-plumes. Both baroclinic (two-and-a-half layer) and barotropic (one-and-a-half layer) models were used. The equations that these two models solve are,

Baroclinic Model:

$$\frac{\partial u_2}{\partial t} - f v_2 = -g' \frac{\partial (h_2 + h_3 + h_b)}{\partial x} + \mathcal{F}_{L2x}, \tag{2.19}$$

$$\frac{\partial v_2}{\partial t} + f u_2 = -g' \frac{\partial (h_2 + h_3 + h_b)}{\partial y} + \mathcal{F}_{L2y}, \tag{2.20}$$

$$\frac{\partial h_2}{\partial t} + H_o \cdot \left(\frac{\partial u_2}{\partial x} + \frac{\partial v_2}{\partial y} \right) = w^*. \tag{2.21}$$

$$\frac{\partial u_3}{\partial t} - f v_3 = -g' h_3 \frac{\partial (h_2 + 2h_3 + 2h_b)}{\partial x} + \mathcal{F}_{L3x}, \tag{2.22}$$

$$\frac{\partial v_3}{\partial t} + f u_3 = -g' h_3 \frac{\partial (h_2 + 2h_3 + 2h_b)}{\partial y} + \mathcal{F}_{L3y}, \tag{2.23}$$

$$\frac{\partial h_3}{\partial t} + (H_o - h_b) \cdot \left(\frac{\partial u_3}{\partial x} + \frac{\partial v_3}{\partial y} \right) = -w^*. \tag{2.24}$$

Barotropic Model:

$$\frac{\partial u_3}{\partial t} - f v_3 = -g' \frac{\partial (h_3 + h_b)}{\partial x} + \mathcal{F}_{L3x} \tag{2.25}$$

$$\frac{\partial v_3}{\partial t} + f u_3 = -g' \frac{\partial (h_3 + h_b)}{\partial y} + \mathcal{F}_{L3y} \tag{2.26}$$

$$\frac{\partial h_3}{\partial t} + (H_o + h_b) \cdot \left(\frac{\partial u_3}{\partial x} + \frac{\partial v_3}{\partial y} \right) = -w^* \tag{2.27}$$

where $\vec{\mathcal{F}}_L$ is the linearized dissipation term:

$$\vec{\mathcal{F}}_L 2 = \frac{A_H}{H_o}\nabla \cdot (H_o \nabla \vec{u}_3) + w^* \frac{\vec{u}_3}{H_o}\Theta(-w^*). \tag{2.28}$$

$$\vec{\mathcal{F}}_L 3 = \frac{A_H}{H_o - h_b}\nabla \cdot ((H_o - h_b) \nabla \vec{u}_3) + w^* \frac{\vec{u}_3}{H_o - h_b}\Theta(-w^*). \tag{2.29}$$

2.2 Basic theory

The basic theoretical methods that will be used later in the thesis will be described in this section. Only layer 3 will be focused on here, but equations for layer 2 can be derived by substituting $-w^*$ for w^* and subscript 2 for 3.

Scaling

Using the momentum equations and the continuity equation, the PV equation in layer 3 is,

$$\frac{dq_3}{dt} = \frac{q_3 w^*}{h_3} + \frac{\mathfrak{F}_3}{h_3}, \tag{2.30}$$

where $q = (f + \zeta)/h$ is the PV and $\mathfrak{F}_3/h_3$ is the PV dissipation defined as the curl of vorticity dissipation

$$\mathfrak{F}_3 \equiv \hat{\kappa} \cdot \nabla \times \mathcal{F}_3. \tag{2.31}$$

over layer thickness where $\hat{\kappa}$ is the unit vector in vertical direction and ζ is the vertical component of the relative vorticity, $\hat{\kappa} \cdot (\nabla \times \vec{u})$.

If steady and linear, Eq 2.30 becomes

$$\beta v_3 = f\frac{w^*}{h_o} + \mathfrak{F}_L, \tag{2.32}$$

where $\mathfrak{F}_L$ is the linearized dissipation term and h_o is the initial layer thickness. If friction is further negligible, this equation becomes the linear vorticity balance equation mentioned previously as Eq 1.1.

If the flow is unsteady and nonlinear, the full PV equation (Eq 2.30) needs to be considered. Decomposing the terms in Eq 2.30 and multiplying it with h_3,

$$\underset{(i)}{\frac{\partial \zeta_3}{\partial t}} + \underset{(ii)}{\vec{u}_3 \cdot \nabla \zeta_3} + \underset{(iii)}{\beta v_3 - \frac{f+\zeta_3}{h}\vec{u}_3 \cdot \nabla h_3} = \underset{(iv)}{\frac{f}{h_3}w^*} + \underset{(v)}{\frac{\zeta_3}{h_3}w^*} + \mathfrak{F}_3. \tag{2.33}$$

The nonlinearity of this equation can be diagnosed by comparing the order of the nonlinear terms to the linear terms. Assumptions will be made here so that geostrophy

is valid ($f \gg \zeta$) and that the linear terms (terms (ii) and (iv)) are still the two main balancing terms in Eq 2.33. From these assumptions, term (v) becomes negligible because $f \gg \zeta$ and the size of other nonlinear terms (terms (i) and (iii)) compared to the linear terms can be estimated in two parameters:

$$\frac{(i)}{(ii)} = \frac{U_3}{\beta L^2} \tag{2.34}$$

$$\frac{(iii)}{(ii)} = \frac{f^2(U_2 - U_3)}{\beta g' H}. \tag{2.35}$$

where U,L and H are the scales for horizontal velocity, horizontal length and layer thickness respectively. Thermal wind balance was used for deriving the second parameter (Eq 2.35.) If these parameters are of order one or larger, the assumption of linear vorticity balance fails.

Barotropic can exist in a nonlinear system. A necessary condition for barotropic instability for a purely zonal flow in a flat bottom is the change of sign in the meridional vorticity gradient. Since the planetary vorticity gradient β is always positive, this condition requires the total vorticity gradient to be negative at some point.

$$\beta - \frac{\partial^2 u_3}{\partial y^2} < 0 \tag{2.36}$$

Non-zonal flows are known to be more easily unstable than this condition but here this condition is used as a rough measure for the potential existence of barotropic instability. When this necessary condition for barotropic instability is met, the parameter in Eq 2.34 is of order one or bigger. If bottom topography is included in the model the condition becomes

$$\beta + \beta^* - \frac{\partial^2 u_3}{\partial y^2} < 0 \tag{2.37}$$

where β^* is the topographic β defined as,

$$\beta^* = \frac{f}{H_o} \frac{\partial h_b}{\partial y} \tag{2.38}$$

Baroclinic instability can also happen in a nonlinear system. The necessary condition for baroclinic instability for a purely zonal flow in a two layer channel model is to have a different sign of PV gradient somewhere in the layer. For a zonally uniform geostrophic flow this condition can be expressed by the velocity shear between the layers that is required to change the sign of the PV gradient. Since the planetary PV gradient is positive, this condition requires PV gradient to be negative at some point;

$$\begin{aligned}
\frac{\partial q_3}{\partial y} &= \frac{\partial}{\partial y}\left(\frac{f+\zeta_3}{h_3}\right) = \frac{1}{h_3}(\beta + \frac{\partial \zeta_3}{\partial y} - \frac{f+\zeta_3}{h_3}\frac{\partial h_3}{\partial y}) \\
&= \frac{1}{h_3}(\beta - \frac{f}{h_3}\frac{\partial h_3}{\partial y}) \quad (\because \text{Zonally uniform } \zeta_3 = 0) \\
&= \frac{1}{h_3}(\beta - \frac{f^2(u_2-u_3)}{g'h}) < 0 \quad (\because \text{Geostrophy})
\end{aligned}$$

therefore,

$$u_s = u_2 - u_3 > \frac{\beta g' h}{f^2} = u_c. \tag{2.39}$$

When u_s, the velocity shear between the layers, exceeds the critical shear u_c, the necessary condition for baroclinic instability is met. This condition was used as a rough estimate to examine the potential for baroclinic instability. It does not exactly hold for non-zonal flows but since non-zonal flows are generally unstable in weaker velocity shear than u_c, so the flow is likely to be already baroclinically unstable when this condition is met. The condition, $u_s > u_c$, is equivalent to having the parameter in Eq 2.35 of order one or bigger.

Thickness balance (Mass conservation)

Reynolds decomposition will be used for velocity and layer thickness separating the variable into a mean term and a fluctuation term,

$$a = \overline{a} + a', \quad \text{where} \quad \overline{a} = \frac{1}{T}\int_0^T a dt \quad \text{and} \quad \overline{a'} = 0. \tag{2.40}$$

where $\overline{a}$ symbolizes the mean and a' the fluctuation term. The continuity equation for layer 3 (Eq 2.6) can be rewritten as,

$$\nabla \cdot \left(\overline{\vec{u}_3}\,\overline{h}_3\right) \quad + \nabla \cdot \left(\overline{\vec{u}'_3 h'_3}\right) \quad = w^*. \tag{2.41}$$

This is the thickness balance equation. The equation shows the balance between mean thickness divergence, eddy thickness divergence, and cross isopycnal velocity. By taking an area integral over some arbitrary area $\mathfrak{A}$, Eq 2.41 can be written as,

$$\oint_c \left(\overline{\vec{u}_3}\,\overline{h}_3\right) \cdot \vec{n} dl + \oint_c \left(\overline{u'_3 h'_3}\right) \cdot \vec{n} dl = \iint_{\mathfrak{A}} w^* dA, \tag{2.42}$$

where $\vec{n}$ is a unit vector perpendicular to the boundary of area $\mathfrak{A}$ and $\oint_c$ is the line integral along the boundary of area $\mathfrak{A}$. This equation shows a balance between the mean transport divergence, eddy transport divergence and the total cross isopycnal transport within area $\mathfrak{A}$.

Potential Vorticity Balance

Using the decomposed form for velocity and potential vorticity (with the same definition of mean and fluctuation as Eq 2.40), the PV equation (Eq 2.30) becomes,

$$\begin{array}{cccc} \overline{\vec{u}_3} \cdot \nabla \overline{q}_3 & + \overline{\vec{u}'_3 \cdot \nabla q'_3} & = \frac{\overline{q_3}}{h_3} w^* & + \frac{\overline{\mathfrak{F}}}{h_3} \\ (a) & (b) & (c) & (d) \end{array} \tag{2.43}$$

Terms (a) and (b) are the mean and the eddy PV advection terms. Terms (c) and (d) are the PV increase by the cross isopycnal flux (PV forcing) term and PV dissipation term. The term "PV balance" is used when the order of each term in this equation is compared. This becomes a very useful way of diagnosing the role of eddies and nonlinearities for it can represent the effect of the two nonlinear terms (terms (i) and (iii)) in Eq 2.33, as one term.

The models described in the first section of this chapter are the ones that will be used in the following two chapters. Table 2.1 summarizes the model parameters

that was used. The second section of this chapter will be used to understand the dynamics of the flow that established in the model calculations. Not only the necessary condition for instability, but the Thickness balance and the PV balance that were described here will become useful for understanding the role of eddies that existed in Figure 1-4.

Case	1	2	3	4
Topography	Flat	Flat	Gaussian	Gaussian
layers	1.5	2.5	1.5	2.5
Basin size (Meridional	400km	400km	600km	600km
× Zonal)	× 800km	× 800km	× 800km	× 800km

Table 2.1: Difference in the model configurations for each case. All other parameters are the same for every experiment, i.e., $A_H = 5\ [m^2 s]$, $\Delta x = \Delta y = 2$ [km], $g' = 5 \times 10^{-4}\ [ms^{-2}]$, and $H_o = 500$ m.

Chapter 3

Numerical Model Result: The effect of Nonlinearity in a flat bottom basin

A linear β-plume in a flat bottom basin is shown in Figure 1-2 has been well studied, but nonlinearity and topographic variation apparently have major effects on β-plume dynamics and can create a complicated flow field as shown in Figure 1-4. In order to understand the dynamics of this flow field, the effects of baroclinicity and topographic variation were studied separately. The effect of nonlinearity using a flat bottom basin, is described in this chapter. The effect of topographic variation is described in the next chapter. All experiments in this chapter and the next use a forcing strength of $w_o^* = 1 \times 10^{-6}$ m/s (equivalent to 0.008 Sv of cross isopycnal transport between the layers).

3.1 Barotropic β-plume: Case 1

Before examining the nonlinear baroclinic β-plume, the nonlinear barotropic β-plume will be examined (Case 1) in order to see how nonlinearity changes the circulation from the linear solution for a barotropic circulation. A one-and-a-half layer model was used and thus the lowest layer (layer 3) is the only moving layer. The term

'barotropic' refers to the flow in the one-and-a-half layer model and 'baroclinic' refers to the flow in the two-and-a-half layer model to distinguish the two types of flow.

After 30 years of spin up, a cyclonic β-plume established [Figure 3-1a]. The circulation was steady except at the southwest corner of the circulation where the western boundary flow separated from the western boundary. A strong meandering was also observed in this part of the circulation. The unsteadiness of the southwest corner and the wavy feature will be examined more closely later in this section.

The cyclonic structure is similar to the linear solution [Figure 1-2b]. The northward flow in the forcing region, zonal jets, and the southward western boundary layer flow remain the same. Maximum horizontal velocity in the forcing region was 0.007 m/s and the transport was 0.28 Sv which are both similar to the linear solution (0.008 m/s, 0.32 Sv). Figure 3-2a shows the size of the terms in the vorticity equation (Eq 2.33) along cross section A (see Figure 3-1a). Although the relative vorticity advection term and the layer thickness advection term [term(i) and (iii)] are not negligible compared to the linear terms [terms (ii) and (iv)], the figure shows that the balance still between the two linear terms.

The unsteadiness at the southwest corner of the β-plume is due to barotropic instability. The necessary condition for this instability is that the vorticity gradient change sign (Eq 2.36). The meridional vorticity gradient in Figure 3-3 shows that the gradient does change sign where the flow was unsteady. The unsteadiness was a slow meridional oscillation and breaking of the wavy feature in this region. This unsteadiness can be seen in Figure 3-1a and b which are a two snapshot of the flow after 30 and 35 years of spinup. The existence of this unsteady southwest corner depended on the magnitude of the velocity of the zonal jet. Experiments with weaker zonal jets had a steady circulation. However, the waviness still existed in those experiments. The waviness, therefore, is not a result of the barotropic instability.

The major difference between this nonlinear result (Figure 3-1) and the linear result (Figure 1-2) is the existence of the waviness in the southern eastward zonal jet. The waviness starts from the western boundary where the western boundary flow overshoots to the south and then gradually dissipates as the flow enters the interior.

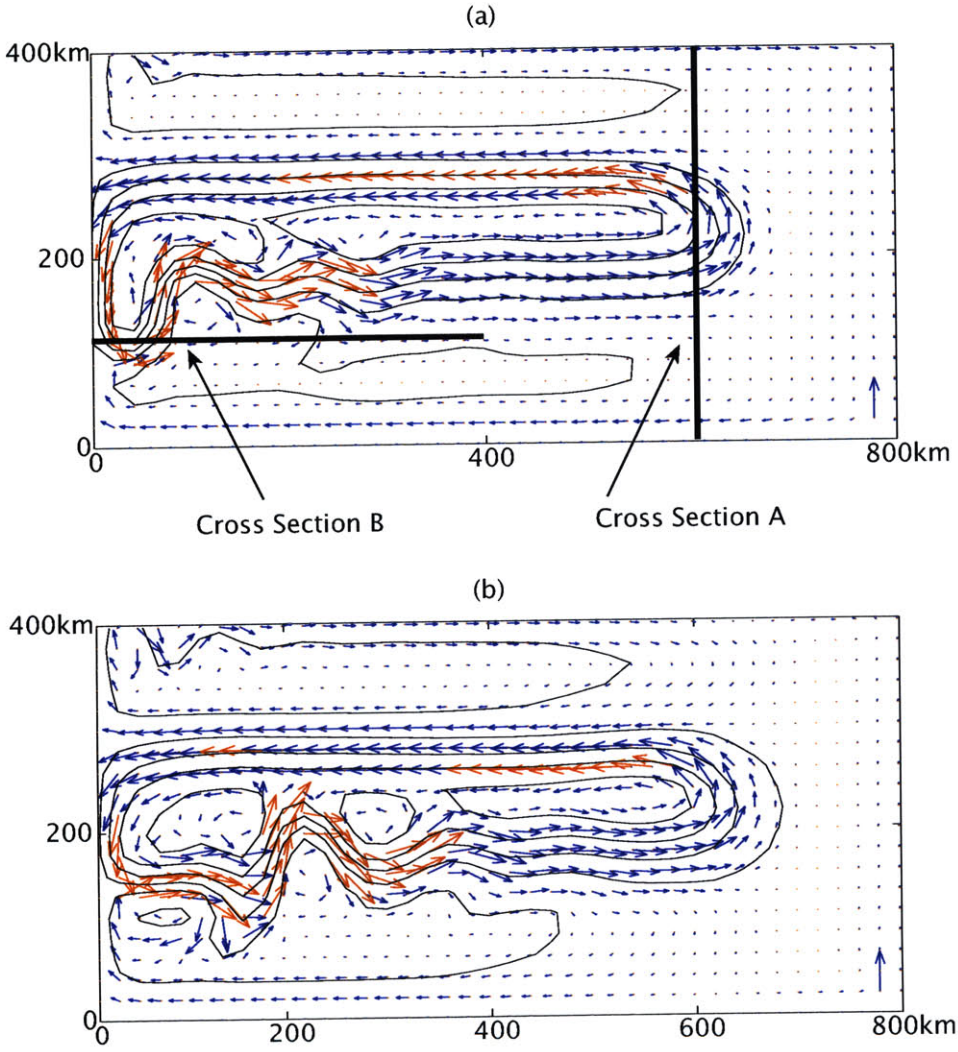

Figure 3-1: Case 1: Barotropic flat bottom β-plume is shown. The plots show the velocity field at a different time with the pressure contour plotted in the background. (a) shows after 30 years of spin up and (b) shows 35 years. Notice that the waviness exists for both cases but the flow is changing its course after it separates from the western boundary. This was the region where the necessary condition for barotropic instability was met. Except for the wavy southwest corner, the structure is similar cyclonic circulation as the linear solution in Figure 1-2. Velocity vectors larger than 0.01 m/s are truncated and are shown in red. For scaling, 0.01 m/s is shown in the down right corner. The two cross sections A and B will be used later.

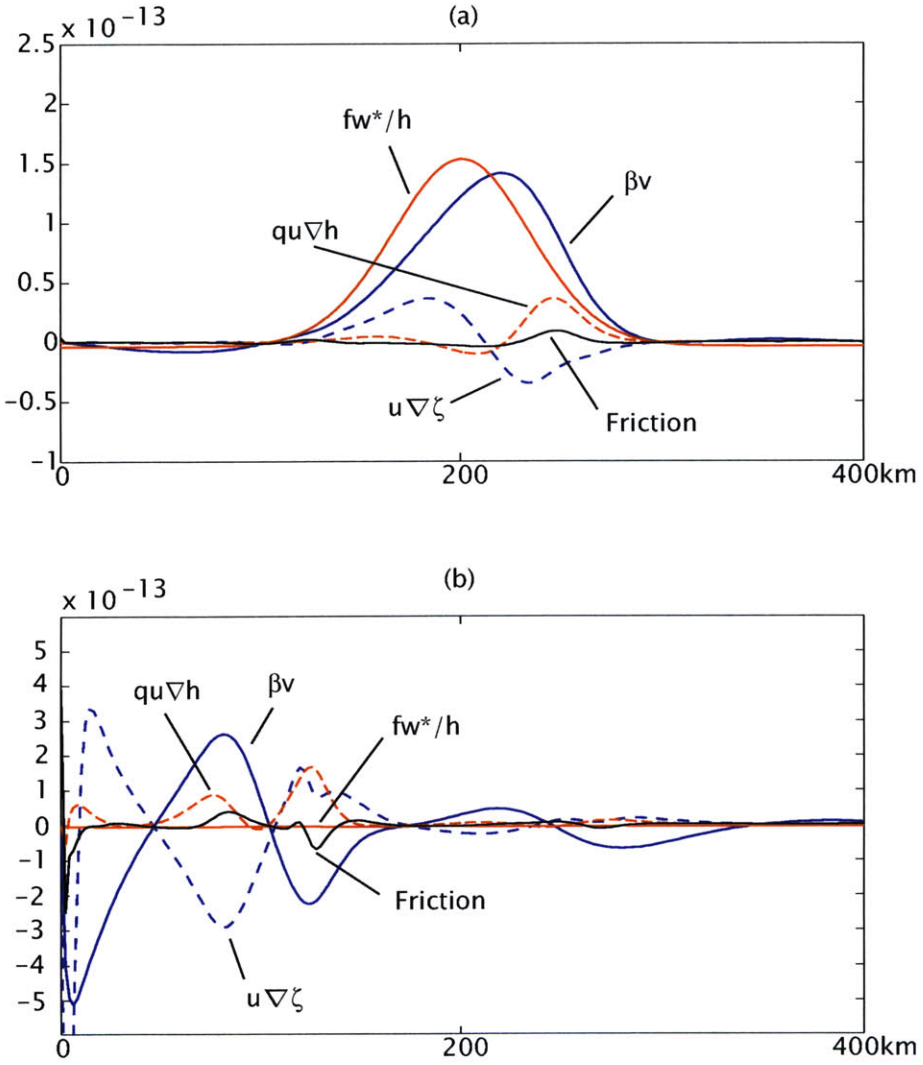

Figure 3-2: Vorticity balance of a barotropic nonlinear case with a flat bottom (Case 1). The plot shows each of the terms in the Vorticity Equation (Eq 2.33) at:
(a) cross section A: The main balance is between the two solid lines. βv and fw^*/h which are the two linear terms in the vorticity equation.
(b) cross section B: The main balance is between βv and $u\nabla\zeta$ in the interior where the waviness exist. The waviness gradually decreases as the flow departs from the western boundary. Friction becomes important in the balance near the western boundary.

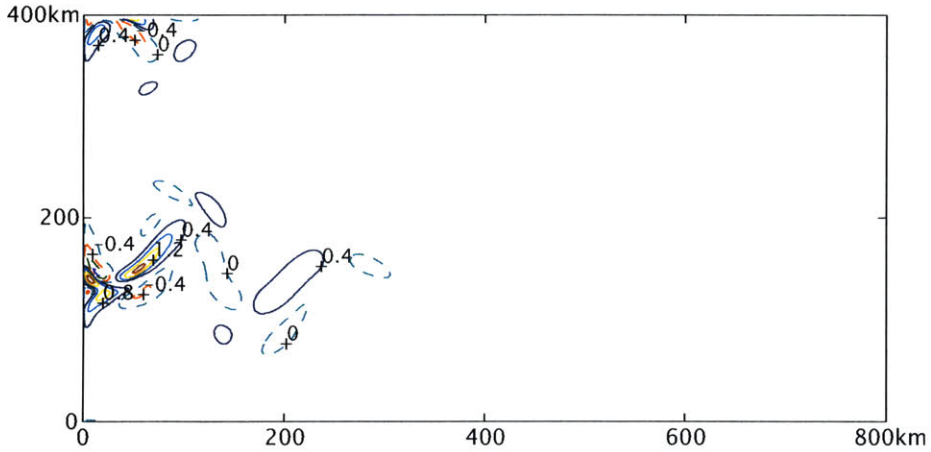

Figure 3-3: Meridional vorticity gradient $\beta - \frac{\partial^2 u}{\partial y^2}$ [1/ms] of a barotropic β-plume in a flat basin (Case 1). The values on the contour are multiplied by 10^{10} for clearer view of the figure. Solid lines represents regions where the meridional gradient is positive and region within the dotted lines represents regions where the meridional gradient is zero or negative. The region closed with the dotted lines have negative gradient. The figure shows region positive gradient and negative gradient closer to the western boundary which matches with the region where the zonal jet separated from the western boundary. The dotted regions near the western boundary shows that the vorticity gradient are negative there, therefore these region satisfies the necessary condition for barotropic instability.

Except for the region where the flow was barotropically unstable, the waviness was steady and did not have any phase propagation. This waviness appears when the inertial boundary layer width ($\delta_I = \sqrt{u/\beta}$) is larger than the Munk boundary layer width ($\delta_M = (A_H/\beta)^{\frac{1}{3}}$). Using the linear vorticity balance in the forcing region to estimate the horizontal velocity scale u, the inertial boundary layer width can be estimated as 100 km wide which is much larger than the Munk boundary layer width 6km. This condition for the existence of the waviness can be expressed in terms of the forcing;

$$\begin{aligned} \left(\frac{A_H}{\beta}\right)^{\frac{1}{3}} &< \sqrt{\frac{u}{\beta}} = \sqrt{\frac{fw_o}{\beta^2 H}} \quad \text{(Linear vorticity balance)} \\ \therefore w_o &> \left(\frac{A_H}{\beta}\right)^{\frac{2}{3}} \frac{\beta^2 H}{f_o} = 1.1 \times 10^{-7} m/s \end{aligned} \tag{3.1}$$

where the initial layer thickness was used for layer thickness scale H. Forcing in this experiment was $w_o = 1 \times 10^{-6}[m/s]$ which does exceed this required minimum for the existence of waviness. The waviness is a standing Rossby wave which has a westward phase speed that is exactly the opposite of the eastward background flow. The existence of a standing Rossby wave is typical for a flow that is inertial, eastward, and strong enough for friction to play role [e.g. *Moore (1964), Cessi (1990)*]. Figure 3-2b shows the size of each term in the vorticity Equation (Eq 2.30) along Cross section B (see Figure 3-1). The plot shows that the wave is created between the relative vorticity advection term and planetary vorticity advection term. The wavenumber of the standing Rossby wave is

$$k = \sqrt{\frac{\beta}{u_{jet}}} \tag{3.2}$$

for a zonal current of u_{jet} [*Pedlosky (1987)*]. Assuming the zonal jet has a zonally uniform velocity, an analytical solution for the wave can be solved from Eq 2.33. The relative vorticity advection term [term (i) in Eq 2.33] is included in a linearized form

by decomposing the terms into the background flow and its perturbation.

$$u \cdot \nabla u \sim u_{jet} \cdot \nabla u'$$

where u' is the velocity of the perturbed field. Using Ψ for the perturbed streamfunction, the steady linear vorticity equation can be solved as,

$$A_H \Psi_{xxxx} \quad -\beta \Psi_x - u_{jet} \Psi_{xxx} = 0 \tag{3.3}$$

$$\therefore \qquad \Psi = \Psi_o exp\left(I\sqrt{\frac{\beta}{u_{jet}}}x\right) exp\left[-\frac{1}{2}\left(\frac{\delta_M}{\delta_I}\right)^3 \frac{x}{u_{jet}^2 \delta_I}\right] \tag{3.4}$$

which gives the dissipation length scale,

$$l = \frac{u_{jet}^2}{\beta A_H}$$

Using the linear vorticity balance equation in the forcing region for the scale of u_{jet} (0.007 m/s), the wavelength can be estimated as 120km with a dissipation length scale of 500km from the western boundary. This theoretically estimated wavelength and dissipation length scale does match with the model result. The linear vorticity balance will remain valid in the forcing region as long as the forcing region is away from the western boundary than this dissipation length.

3.2 Baroclinic β-plume: Case 2

Baroclinicity was then added to the previous experiment by using a two-and-a-half layer model (Case 2).

The flow did not reach a steady state, but after 50 years of spin up, the flow reached a statistically steady state[1] [Figure 3-4]. A snapshot and the mean[2] of the pressure and velocity field of this final state in layer 2 are shown in Figures 3-5 and 3-6. Corresponding plots for layer 3 are shown in Figures 3-7 and 3-8. The snapshots

[1]The term 'statistically steady state' is used for a state when the time averaged flow field does not change significantly with time.

[2]Mean is taken over the last 100 years of model run.

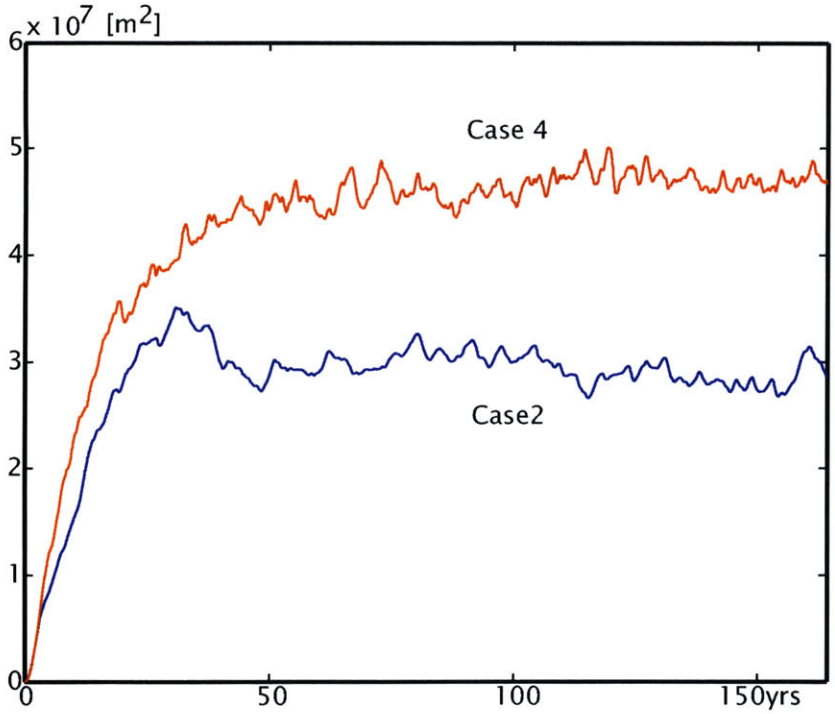

Figure 3-4: Potential Energy (PE) divided by $\rho_o g'$ for two baroclinic cases are shown. PE is integrated for the whole layer over the whole basin: $PE/\rho_o g' = \iint(\eta_2^2 + \eta_3^2)dA$ where η_2 is the height deviation at the interface between layer 1 and 2, and η_3 is for the interface between layer 2 and 3. baroclinic flat bottom case (Case 2) and baroclinic flow with a Gaussian bump (Case 4) reaches a steady state in 50 and 80 years after spinup respectively. Case 4 takes longer time to reach a steady state because of its larger basin size.

in both layers show no particular structure and the whole gyre was dominated by eddies. However, the mean flow resembles a familiar β-plume; the flow is anticyclonic in layer 2 and cyclonic in layer 3 although the flow has become broad and weak compared to experiment 1.

The maximum horizontal velocity of the mean flow in the forcing region was 0.003 m/s for layer 2 and 0.004 m/s for layer 3. The horizontal transport of the zonal jet was 0.06 Sv for layer 2 and 0.08 Sv for layer 3. The magnitude of the transport decreased to roughly a third of the value of case 1 (0.007 m/s, 0.28 Sv). The zonal transport of case 1 and the mean zonal transport of this case at cross section C (see figure 3-8) are compared in Figure 3-9. The decrease of the transport is clear.

Baroclinic instability is the main mechanism for generating the eddies. From Eq

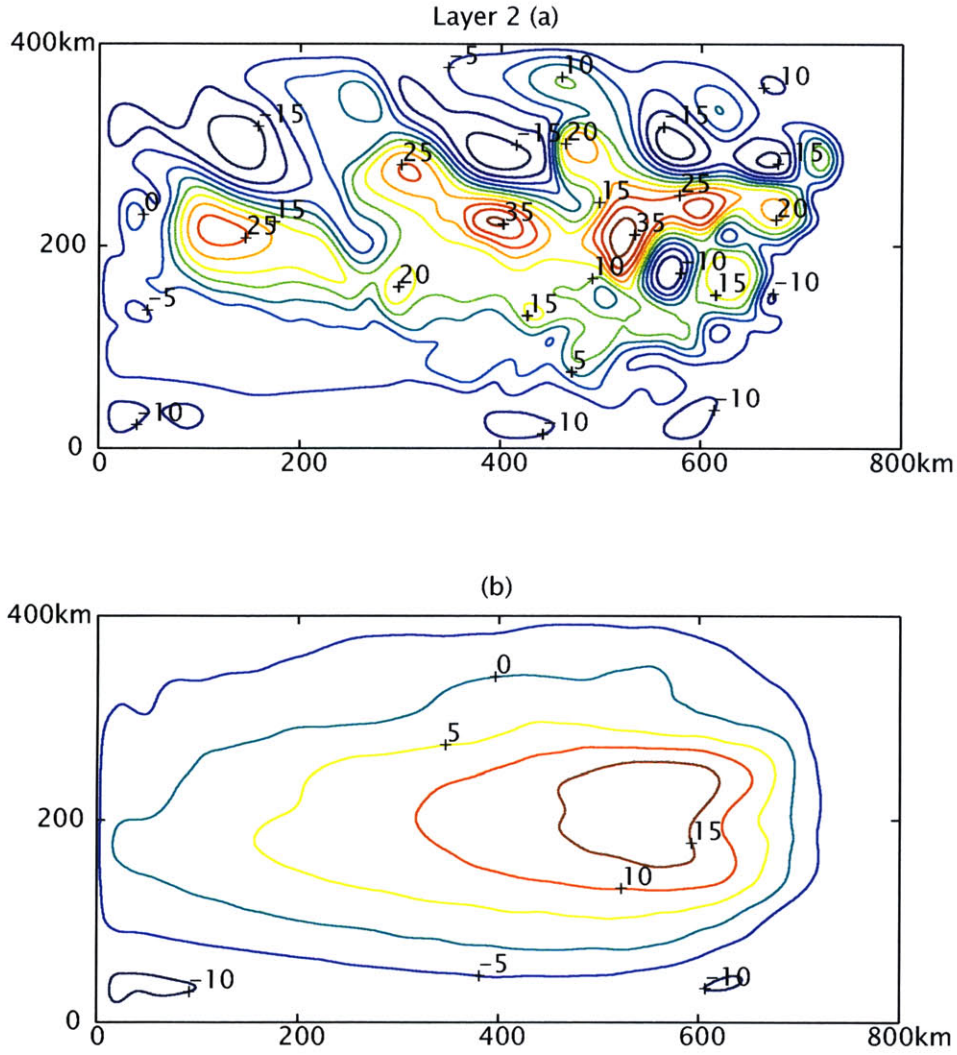

Figure 3-5: Pressure contours in layer 2 for a baroclinic flat bottom case (Case 2). The pressure in this layer is $P_2 = \rho_o g' \cdot (h_2' + h_3')$ and the figure shows $h_2' + h_3'$ where ' represents the fluctuation from initial state. (a) A instantaneous pressure field after 100 years and (b) mean pressure field are shown. Contour intervals are $50[m]$for each plot. (a) The instantaneous pressure field shows a field dominated by eddies. Small eddies are around the forcing region. The eddies become larger as it moves away from the forcing region and are eventually dissipated. β-plume structure can hardly be recognized. (b) The mean pressure field shows a familiar β-plume. The flow is in anticyclonic sense. The interval of the pressure contours are much broader than Case 1 (Figure 3-1). Also pressure gradient exists where it did not in case 1. The figure shows the weakening and broadening of the mean flow.

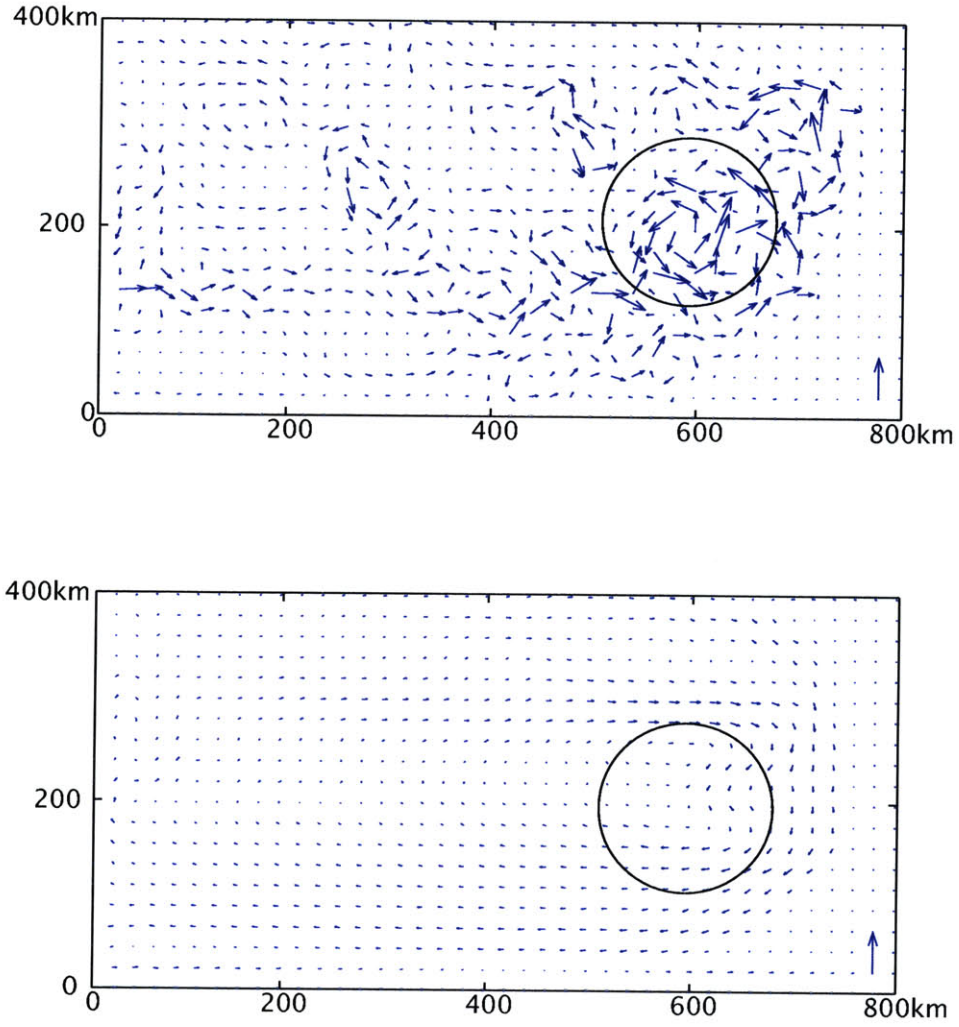

Figure 3-6: Velocity field in layer 2 for a baroclinic flat bottom case (Case 2) The size of the vectors can be compared with Figure 3-1. (a) The instantaneous velocity after 100 years and (b) the mean velocity are shown. Just like the pressure field, (a) shows a field dominated by eddies. They have large velocity values compared to the mean. Small eddies are around the forcing region. The eddies become larger as it moves away from the forcing region and are eventually dissipated. β-plume structure can hardly be recognized. (b) shows a familiar β-plume, although it is very hard to see this because the flow is very weak. The flow is in anticyclonic sense. Velocity vectors exists where it did not in case 1. The figure shows the weakening and broadening of the mean flow. Velocity vectors larger than 0.01 m/s are truncated and are shown in red. For scaling, 0.01 m/s is shown in the down right corner

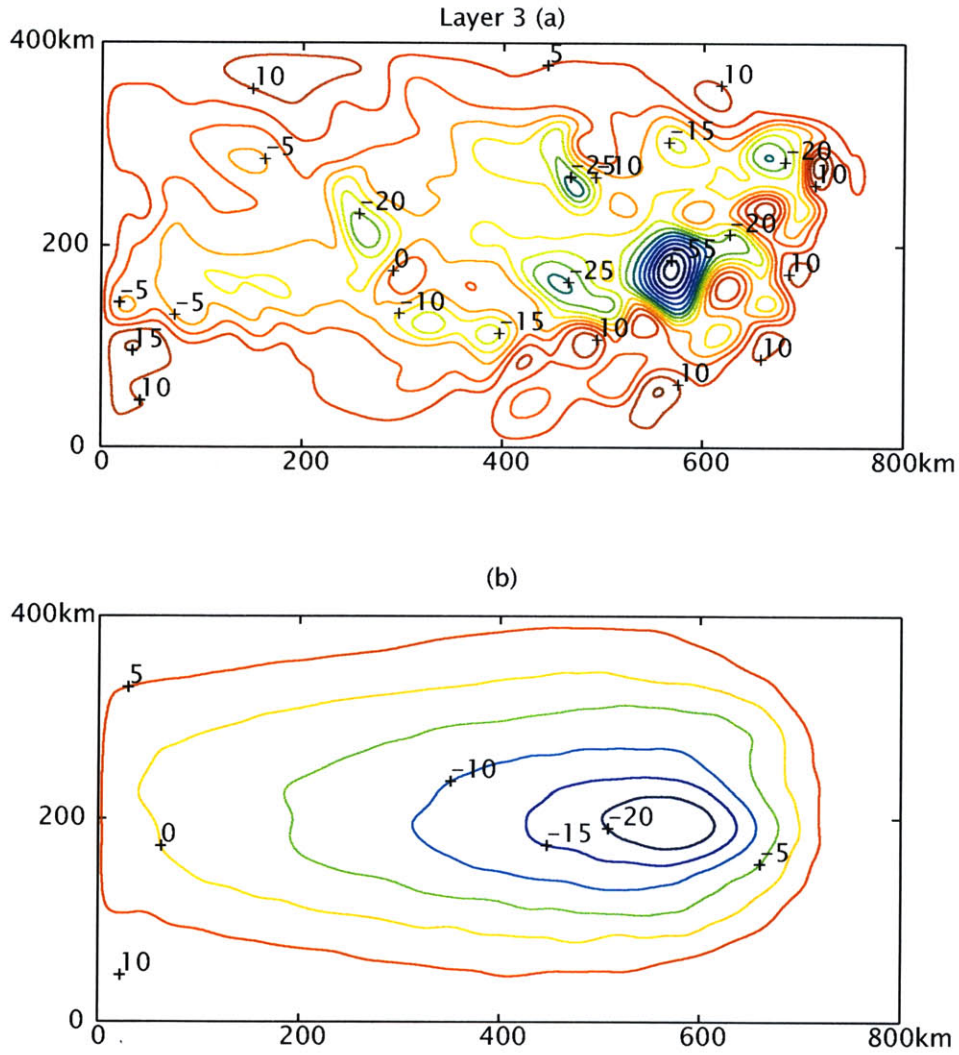

Figure 3-7: Pressure contours in layer 3 for a baroclinic flat bottom case (Case 2) Pressure fluctuation is $P_3 = \rho_o g' \cdot (h_2' + 2h_3')$ in this layer and the values shown in the picture are $h_2 + 2h_3'$. (a) A instantaneous pressure field after 100 years and (b) mean pressure field are shown. The total pressure field (a) represents only one snap shot of the statistically steady state. Contour intervals are $50[m]$for each plot. (a) The instantaneous pressure field shows a field dominated by eddies. Small eddies are around the forcing region. The eddies become larger as it moves away from the forcing region and are eventually dissipated. β-plume structure can hardly be recognized. (b) The mean pressure field shows a familiar β-plume. The flow is in cyclonic sense. The interval of the pressure contours are much broader than Case 1 (Figure 3-1). Also pressure gradient exists where it did not in case 1. The figure shows the weakening and broadening of the mean flow.

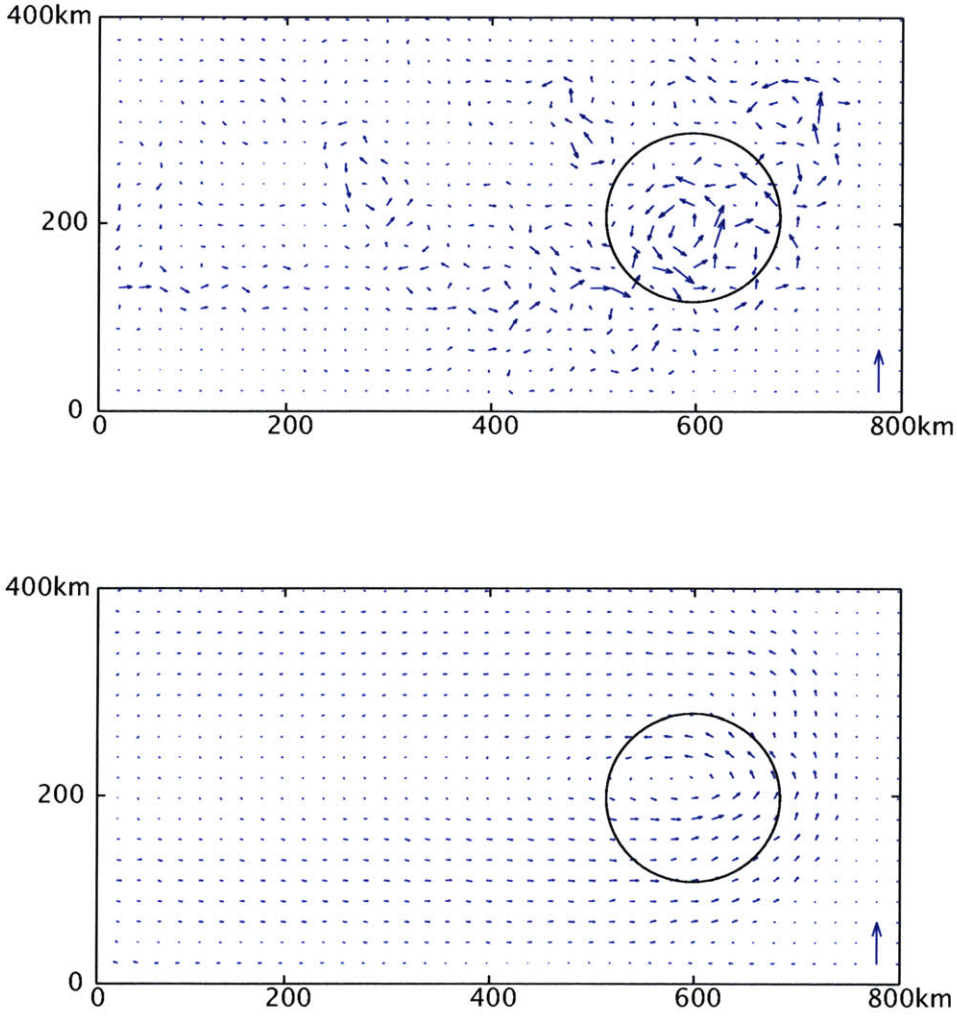

Figure 3-8: Velocity field in layer 2 for a baroclinic flat bottom case (Case 2) The size of the vectors can be compared with Figure 3-6. (a) The instantaneous velocity after 100 years and (b) the mean velocity are shown. Just like the pressure field, (a) shows a field dominated by eddies. Small eddies are around the forcing region. The eddies become larger as it moves away from the forcing region and are eventually dissipated. β-plume structure can hardly be recognized. (b) shows a familiar β-plume although it is hard to see because of the small values. The flow is in cyclonic sense. Velocity vectors exists where it did not in case 1. The figure shows the weakening and broadening of the mean flow. Velocity vectors larger than 0.01 m/s are truncated and are shown in red. For scaling, 0.01 m/s is shown in the down right corner

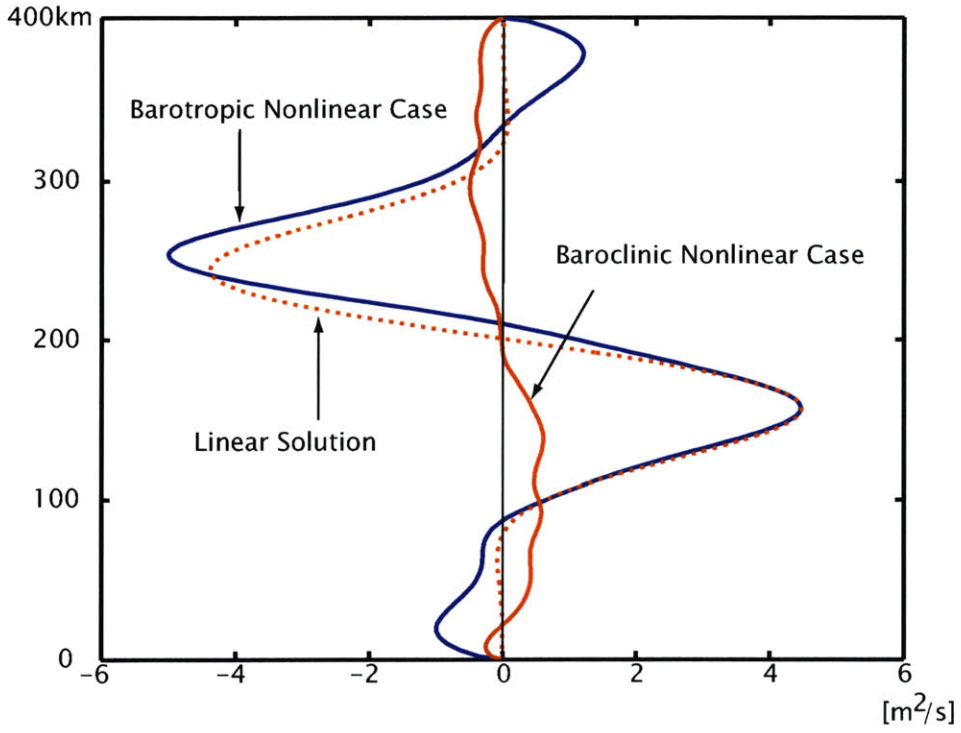

Figure 3-9: Comparison of zonal transport of case 1 and 2 along Cross section C. The values for Case 1 are shown in Blue and the values for Case 2 are shown in Red. Case 1 shows the westward zonal jet in the north ($y \sim 250km$) and eastward zonal jet in the south ($y \sim 150km$). Case 2 shows a decrease of magnitude in both of the jets. It also shows that the zonal jets have diffused out to north and south. The decrease of magnitude between the two experiment is clear.

2.39, the required velocity shear (between the two layers) for baroclinic instability is,

$$u_c = \frac{\beta g' H}{f^2} = \frac{2 \times 10^{-11} \cdot 5 \times 10^{-4} \cdot 500}{(7 \times 10^{-5})^2} = 0.001 \quad m/s. \tag{3.5}$$

The maximum mean velocity shear of the model result was 0.0019 m/s (in the forcing region) which exceeded this critical value. The velocity shear for the whole basin is shown in Figure 3-10a, showing that the criteria is met near the forcing region where eddies formed actively. How the maximum horizontal velocity changed with forcing strength is plotted in Figure 3-10b. The values are also compared to the linear solution. The figure shows the model result departing from the linear solution as the forcing strength increased. This departure from the linear solution is likely the result of baroclinic instability. The reason is as follows. A critical value of w_c^* for the on set of baroclinic instability can be estimated by using the linear vorticity balance for the estimate of the velocity field:

$$u_s = |u_2 - u_3| = \frac{2fw*}{\beta H_o}. \tag{3.6}$$

By comparing this velocity shear to the critical value u_c, the critical value w_c^* can be estimated;

$$u_s > u_c \tag{3.7}$$

$$\therefore w^* = \frac{2\beta^2 g' H_o^2}{2f^3} = 0.7 \times 10^{-8} \mathrm{m}/s \tag{3.8}$$

This critical value $w_c^* = 0.7 \times 10^{-8} \mathrm{m}/s$ matches fairly well with where the model results started to depart from the linear solution. Although the criterion is only valid for zonally uniform flows, non-zonal flows tend to be more unstable than purely zonal flows and this criterion was still useful for a rough estimate for the onset of baroclinic instability. When instability did not occur, the circulation in became similar to the linear case (Figure 1-2) for both layers. The criterion was shown to be useful (but roughly), but a more careful theoretical examination will be needed for an exact criterion for the onset of baroclinic instability.

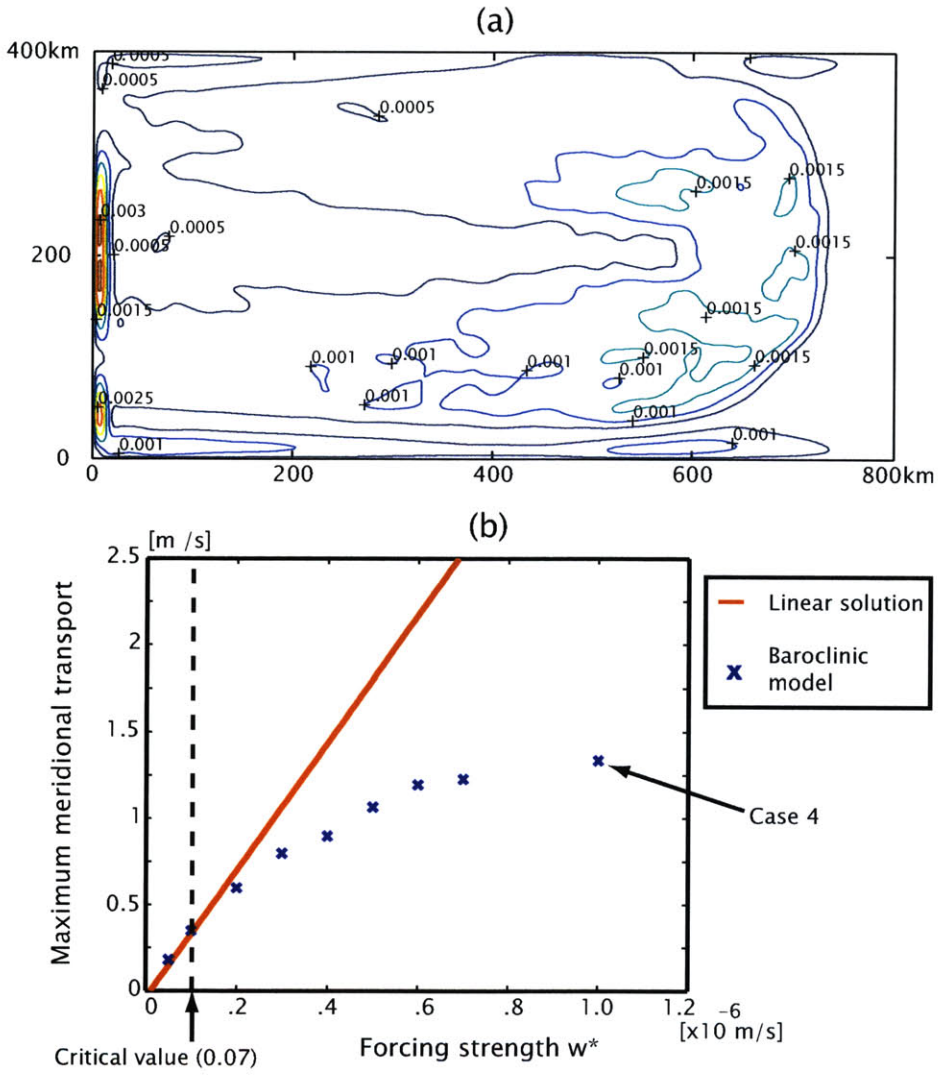

Figure 3-10: The sensitivity of the baroclinic instability criterion is shown for the nonlinear baroclinic case with a flat bottom. (a) shows the velocity shear between the two layers for Case 2. (b) shows the sensitivity of the criterion by comparing w^* and the maximum horizontal transport. The critical value of w^* for the onset of baroclinic instability is 0.07×10^{-6}. The departure of the the model result from the linear solution does seem to match roughly around this critical value.

Baroclinic instability converted the potential energy of the mean flow to the eddies and reduced the velocity shear between the two layers. Eddies in this experiment were generated near the forcing region and were about the size of deformation radius. The eddies eventually propagated to the west and dissipated as they went out of the forcing region. The role of these eddies can be investigated from layer thickness balance (see Chapter 2). Each of the terms in the thickness balance equation for layer 3 (Eq 2.41) are plotted in Figure 3-11. The figure shows a balance between the forcing and the eddy transport divergence in the forcing region. The loss of thickness by the forcing is balanced by the eddy thickness flux from outside the forcing region. The region outside the forcing region (both north and south) shows a balance between the mean and eddy transport divergence. This indicates that the mean flow in this region was driven by eddies. The broadening of the mean flow that was observed in Figure 3-7 or 3-8 can be explained as a result of this eddy activity.

The role of eddies can also be investigated from looking at the PV balance. Figure 3-12 shows the PV balance for layer 3 along cross section A (see Figure 3-1). It shows that the eddy PV flux was a major balancing term with PV forcing. The eddies have taken the role of balancing the PV forcing in a way similar to the layer thickness balance mentioned above. The mean flow driven by the eddies outside the forcing region is also clear from this figure.

Eddies began to play a critical role in the thickness or PV balance when baroclinicity was included into the model. The eddies redistributed layer thickness and PV between the forcing region and its surroundings, making the mean flow weaker and broader than the barotropic case (where there were no eddies, Figure 3-1). Comparing the two cases, the existence of eddies seems to indicate that their existence is somewhat similar to viscosity, i.e., redistributing momentum to the surroundings. It is not difficult to imagine a similar β-plume to establish by having an enhanced viscosity value near the forcing region in the model. The instantaneous flow also resembles the past works on the instability mechanism of two vortices of different sign on top of each other on a f-plane where instability happened all around the forcing region [e.g. *Flierl (1988), Helfrich and Send (1988)*] and numerical studies of a local-

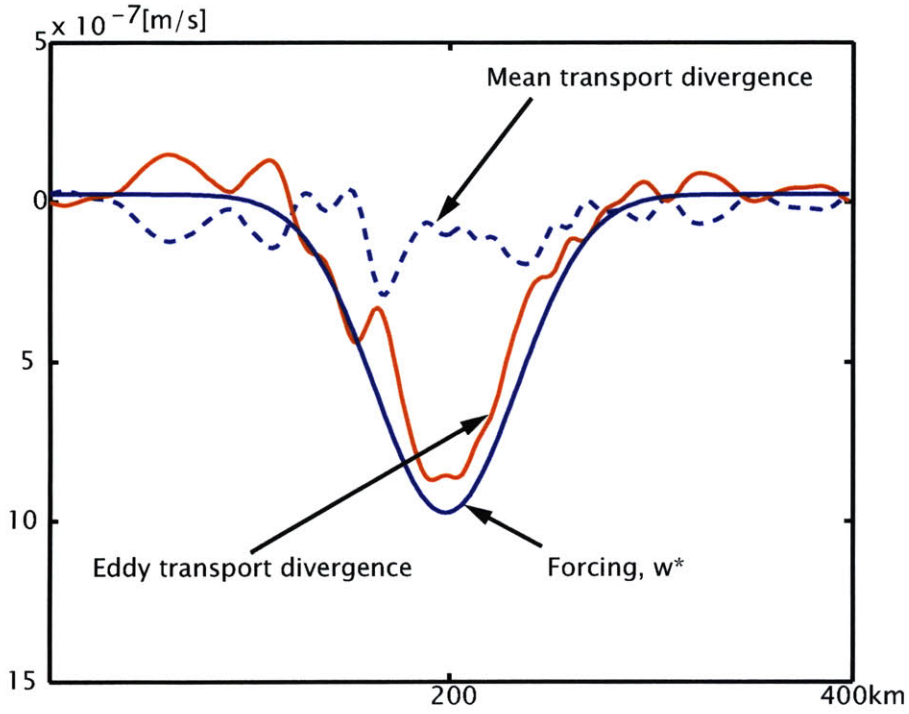

Figure 3-11: Thickness balance of layer 3 in the case with flat bottom and baroclinicity (Case 2): Thickness balance (Eq 2.41) along cross section A is shown in this plot. (This cross section crosses the region of intense cross isopycnal transport from layer 3 to 2.) Eddy transport divergence term (Red) is shown as the major balancing term with the forcing. The mean transport divergence (Dotted) is small compared to the eddy thickness advection in this region. The plot shows a big change from case 1 where the forcing was balanced completely by the mean transport divergence. Outside the forcing shows a balance between the eddy and mean transport divergence. This is an indication that the mean flow in this region was created by the eddies.

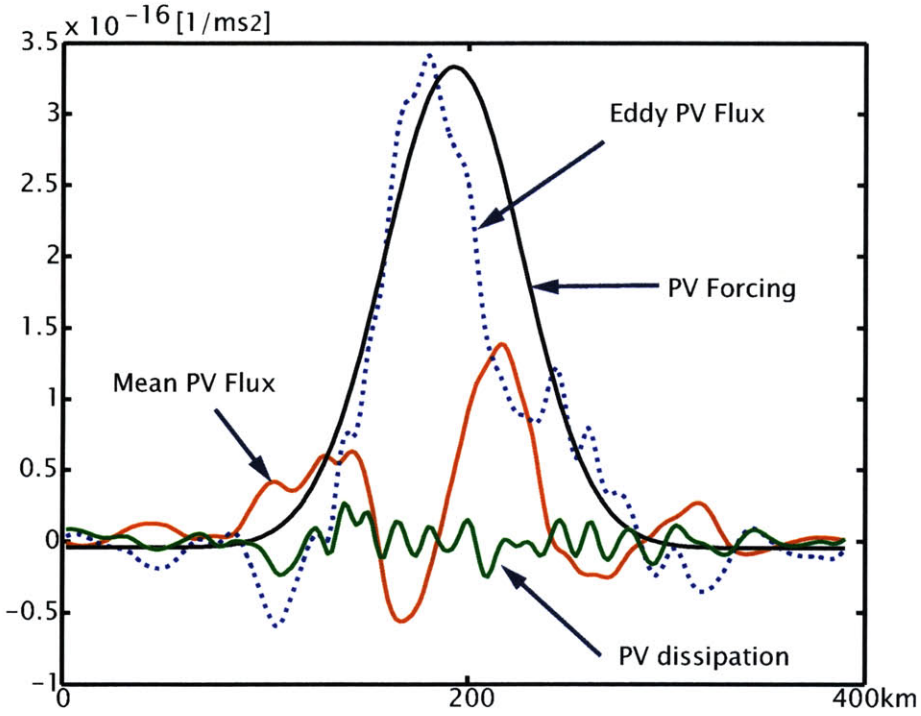

Figure 3-12: PV balance for a baroclinic flat bottom case (case 2): This figure shows the PV balance at cross section A. The PV increase by the intense cross isopycnal velocity is noted as 'PV Forcing'. This plot shows that the PV forcing is balanced by eddy PV flux rather than the mean PV flux. Surrounding the forcing region is a balance between the mean PV flux and eddy PV flux. This indicates that the mean flow in this region driven by the eddies.

ized PV forcing on a f-plane [*Wardle and Marshall (1999)*]. The resemblance seems to be from the fact that eddies existed uniformly around the forcing region for this particular case. However, the importance of the eddies in balancing with the forcing is not uniform around the forcing region although the existence of eddies are uniform. There is a dependence in the direction of where the eddies play an important role or not. Figure 3-13 shows the mean and the eddy transport divergence terms in the thickness balance for the whole basin. (Figure 3-11 is the cross section A of this figure.) It shows that the eddy-mean balance exist only to the east of the forcing region and not to the west. It also shows that the thickness lost in the forcing region, was mainly brought from the eastern side of the forcing and not from the west. The eddies that existed to the west of the forcing region did not have a significant role in balancing with the forcing. The role of eddies, therefore, is not quite the same as enhanced viscosity. The non-uniform behavior of eddies in balancing with the forcing is likely to occur because of the β effect, but to understand exactly where and how this takes place needs more careful examination.

The next chapter will focus on the effect of topography on β-plumes.

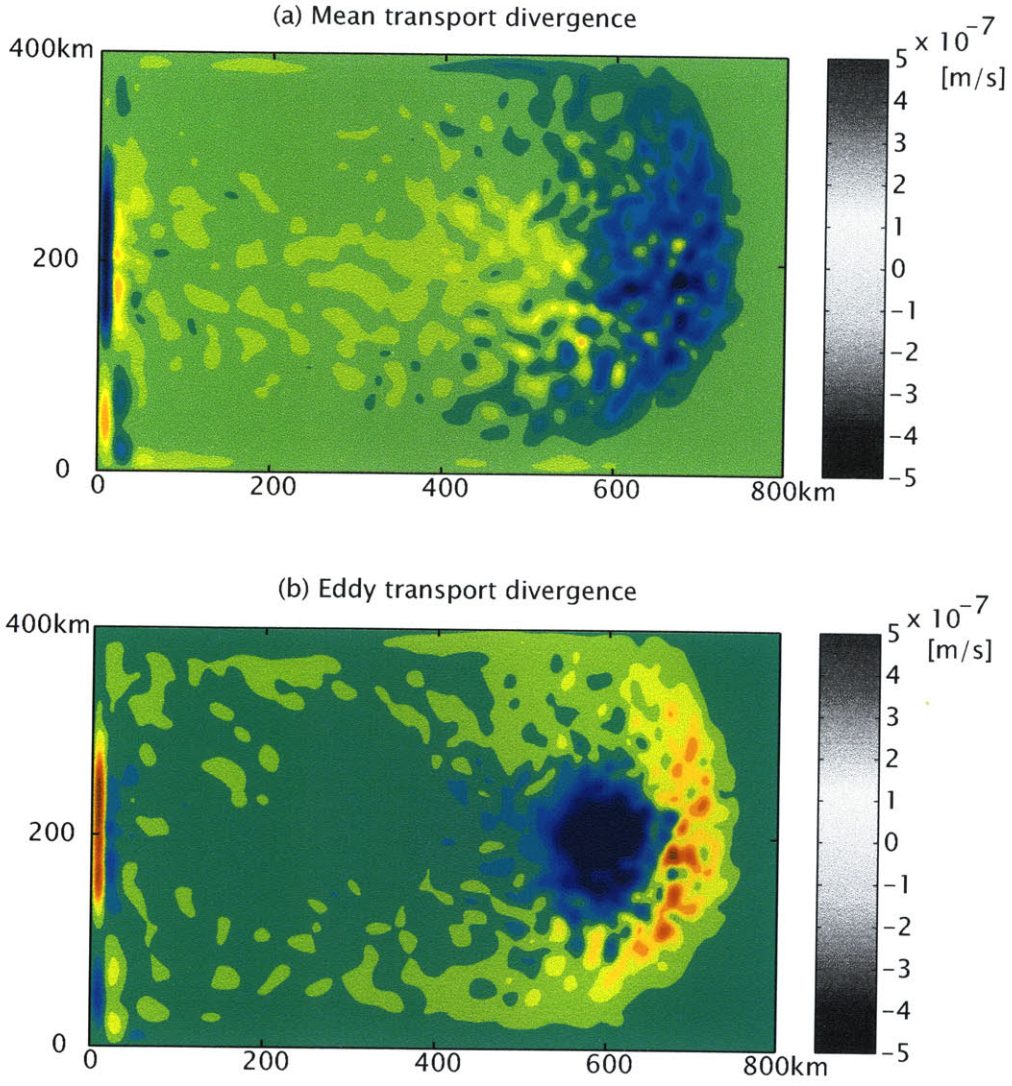

Figure 3-13: Thickness balance for a baroclinic flat bottom case (case 2) in the whole basin: (a) is the Mean transport divergence term and (b) is the Eddy transport divergence term. (Figure 3-11 was a cross section of this plot along cross section A.) (a) shows the spreading of the mean circulation. The term exists outside the forcing term. (b) shows a balance between the forcing in the forcing region. However, outside the forcing region shows a positive eddy transport divergence. This is where the eddy transport divergence balance the mean flow which resulted in the spreading of the mean circulation outside the forcing region. The figure shows that this eddy-mean balance only exist to the eastern half outside the forcing region which is a clear indication of the non-uniform behavior of eddies around the forcing region.

Chapter 4

The effect of bottom topography

The effect of bottom topography is examined in this chapter. Because topographic variation changes the background PV ($f/(H_o - h_b)$), the structure of the β-plume can be altered. The background PV for layer 3 when a Gaussian bump (Figure 2-3, described in chapter 2) is included in the model, is plotted in Figure 4-1. Notice that the gaussian bump created a closed PV contour region. The existence of this closed PV contour region will have a significant impact on the structure of the β-plume in the cases shown in this chapter. Topographic variation will affect the flow not only in layer 3 (which is in direct contact with the bottom topography), but in layer 2 also. This chapter is organized as follows. First, the linear barotropic case will be described. Next, nonlinearity will be included into the barotropic model. Finally, baroclinicity will be included by using the nonlinear baroclinic model. All cases in this chapter will use a forcing strength of $w_o = 1 \times 10^{-6}$ m/s. This forcing strength is the same strength as the previous cases with a flat bottom (Chapter 3).

4.1 Linear Solution

The linear solution was solved using a linear barotropic model described in Chapter 2. Figure 4-2 shows the height deviation from the initial resting state of this solution. The major difference from the linear barotropic flat bottom result (Figure 1-2) is the existence of a strong recirculation around the Gaussian bump. This strong recircula-

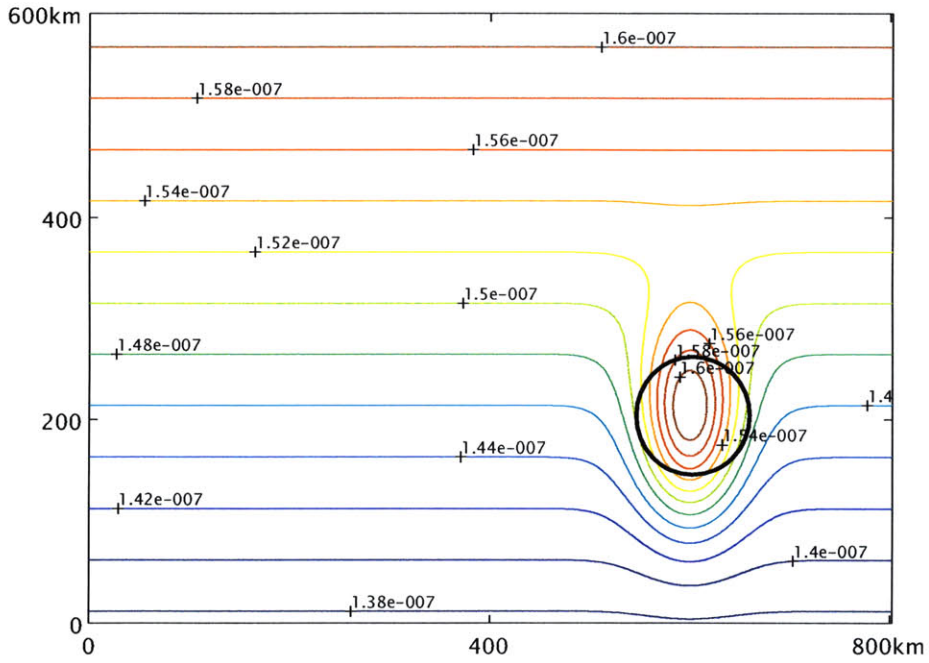

Figure 4-1: The Background PV (f/H_o) for cases with the Gaussian bump for bottom topography. The forcing region is shown with a black circle. There is a region of closed PV contour which is created by the Gaussian bump. This region of closed PV contour coincides with the forcing region, but the rest of the basin shows the PV equivalent to the case with a flat bottom.

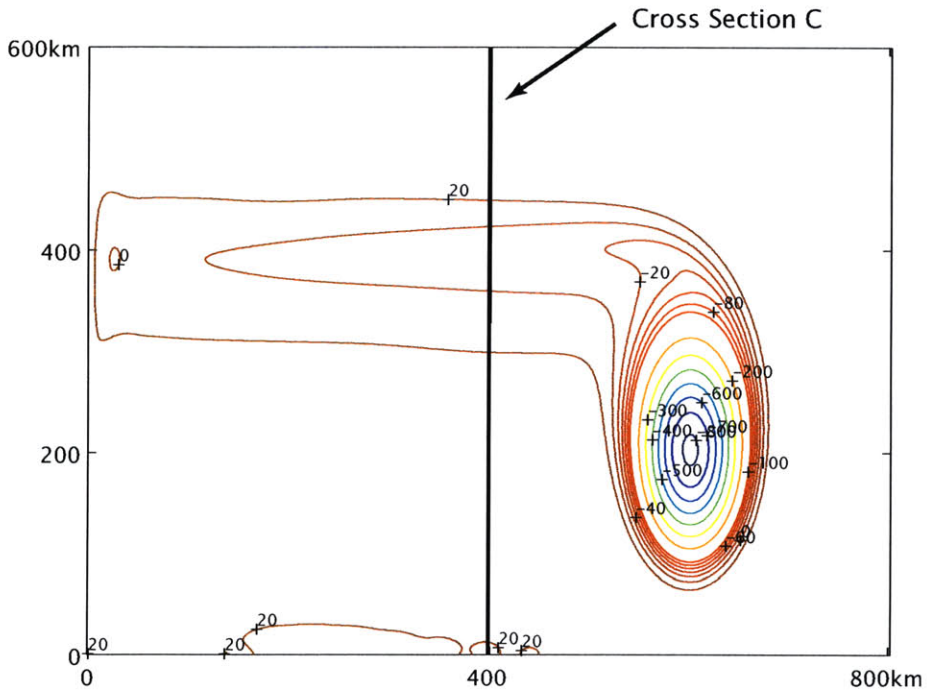

Figure 4-2: The linear solution for the case with the Gaussian bump for bottom topography. The layer thickness deviation from the initial resting state is shown here. The layer thickness field is the same as the the pressure field since $h_3' = P/\rho_o g'[m]$. Note that the contour intervals are irregular. There is a closed contour region with the thickness deviation values extremely negative. This is the region of closed PV contour (Figure 4-1) where friction becomes important for a linear system. The change in the background PV shifted the zonal jets of the β plume northward. The two zonal jets have a weak thickness(pressure) gradient is weaker than the flat bottom case. The contour intervals seems slightly broader for the southern eastward zonal jet than the northern westward jet.

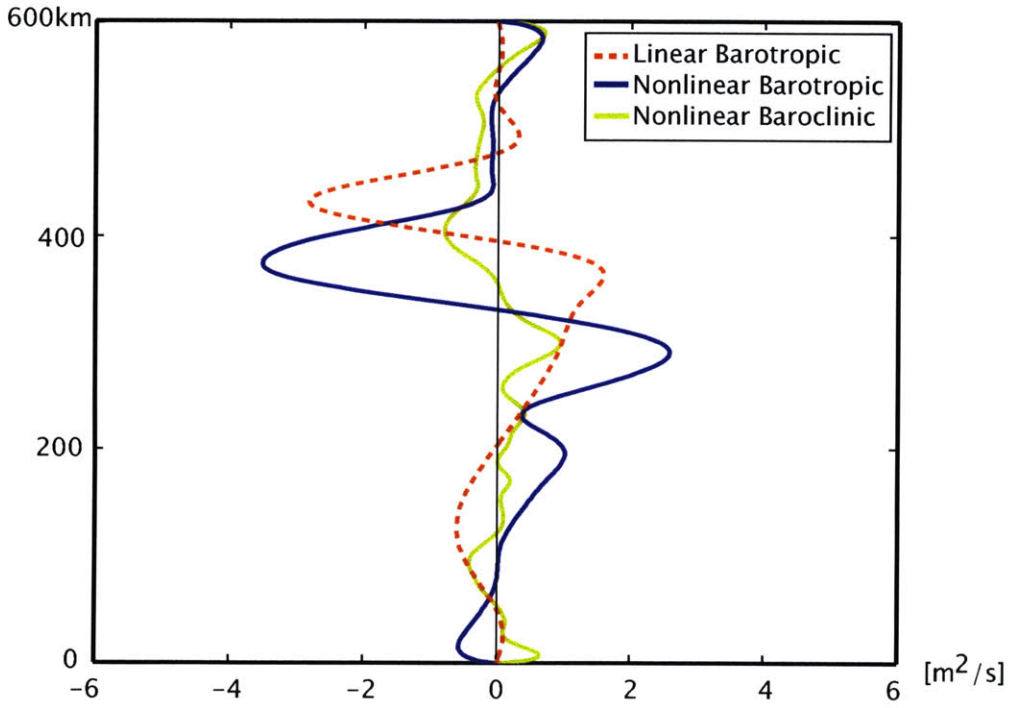

Figure 4-3: The Horizontal transport along Cross section C for cases with the Gaussian bump:
(a) The linear solution is shown in a red dotted line. The two zonal jets in the north ($y \simeq 400km$) are the jets that were shifted by the presence of the Gaussian bump. There is also a westward jet in the south ($y \simeq 100km$) that is weak but significant to play a role in the vorticity balance.
(b) One-and-a-half layer Nonlinear Case (Case 3) is shown in blue solid line. The two zonal jets in the north has shifted southward compared to the linear solution. The strength of the zonal jets have also increased and the southern westward jet that existed in the linear solution disappeared.
(c) Two-and-a-half layer Nonlinear Case (Case 4) is shown in green solid line. The latitude of the two zonal jets are similar to that of Case 3 but the strength have decreased. This decrease is similar to the decrease in the flat bottom case when baroclinicity was included (Figure 3-9).

tion establishes because friction plays the central role in the dynamics of this region. The reason is as follows. The flow must have a net mass transport across a closed PV contour in order to balance the thickness (mass) loss by the forcing. Suppose the flow was steady and friction was negligible. Then the flow is in geostrophic balance. Linearity implies that the effect of relative vorticity or change in layer thickness by the flow is excluded; thus the flow feels only the background PV (f/h_o) where h_o is the initial layer thickness. Defining the layer thickness term as $h = H_o + \eta$ where H_o is the initial layer thickness and η is the thickness deviation, the mass transport across a closed PV contour will be,

$$\oint_{ConstantPV} H_o \vec{u} \cdot \vec{l} dl = \oint g' \frac{H_o}{f} \nabla\eta \cdot \vec{l} dl \quad (\because Geostrophy) \tag{4.1}$$

$$= g' \frac{H_o}{f} \oint \nabla\eta \cdot \vec{l} dl \quad (\because Constant\, PV) \tag{4.2}$$

$$= 0 \tag{4.3}$$

where $\vec{l}$ is the vector along the line integral. This equation implies that geostrophic flow can not have a net transport across a closed PV contour. However, the flow must somehow balance mass so the flow needs to creates an ageostrophic component. The only way that the ageostrophic component can be created is by using friction and this is why friction starts to play the central role in the dynamics of this closed PV contour region. The intense recirculation was created so that friction term can become important in the momentum balance. The recirculation in this linear case had a maximum horizontal velocity of 0.12 m/s and a transport of 3 Sv which is about an order of magnitude stronger than in the previous cases. In fact, the recirculation was so strong that the total layer thickness became negative. Obviously the assumption of linearity was inappropriate for this case.

The strength of the zonal jet have weakened compared to the flat bottom case. The maximum velocity was 0.005 m/s and the transport was 0.12 Sv for the westward jet. This decrease of zonal jet is from topographic β effect. Eq 1.3 shows the ratio of horizontal transport to the cross isopycnal transport. Because the effective β from topography is large in this experiment, topographic β needs to be used instead of

the planetary β. Effective β was few times larger than the planetary β and thus decreased the magnitude of the flow. The zonal transport along cross section C is shown in Figure 4-3. Besides the two zonal jets in the north, a weak southern zonal jet also existed. Although this zonal jet is an interesting feature and is necessary to close the total PV budget[1], the two more familiar zonal jets in the north will be the main focus here and in the following sections.

4.2 Barotropic β-plume: Case 3

The effect of nonlinearity is examined by using a nonlinear barotropic model (Case 3). Bottom topography, forcing strength and other model parameters are the same as in the previous linear case [Table 2.1].

The flow does not reach a steady state but reaches a statistically steady state. Figure 4-4a shows a snapshot of the velocity field of this final state and Figure 4-4b shows the time mean velocity field. The flow created a strong cyclonic mean circulation along the Gaussian bump like the linear solution but the maximum mean velocity and the transport were 0.02 m/s and 0.34 Sv which are an order of magnitude smaller than the linear case (0.12 m/s, 3 Sv). There was also an asymmetry between the recirculation flow in the north and south of the bump whereas the linear case did not. The maximum mean velocity north of the bump was 0.003 m/s which is weaker than the south (0.01 m/s) and the eddies were also present and existed more to the north.

The zonal jet had a maximum velocity of 0.01 m/s and a transport of 0.20 Sv. The cross section of the zonal transport is shown in Figure 4-3. Compared to the linear

[1]The Total PV budget is meant for the total PV balance over the forcing region. (In general, this can be any arbitrary area) Taking an area integral of the vorticity equation,

$$\oint_c \left(\vec{U}\cdot\vec{n}\right)\left(\frac{f+\zeta}{h}\right)dl = \int\int_A \nabla\times\mathfrak{F}dA = \oint_c \mathfrak{F}\cdot\vec{n}dl \tag{4.4}$$

where the line integral c is around the area of where the integral was taken. The dissipation term can assumed to be negligible if the line integral is in the interior far enough from the forcing region or the lateral boundaries, so the RHS of the equation is zero. This means that there are no total vorticity input into the area that the integral was taken. This zero input of total vorticity was the total PV budget that was checked with the model result.

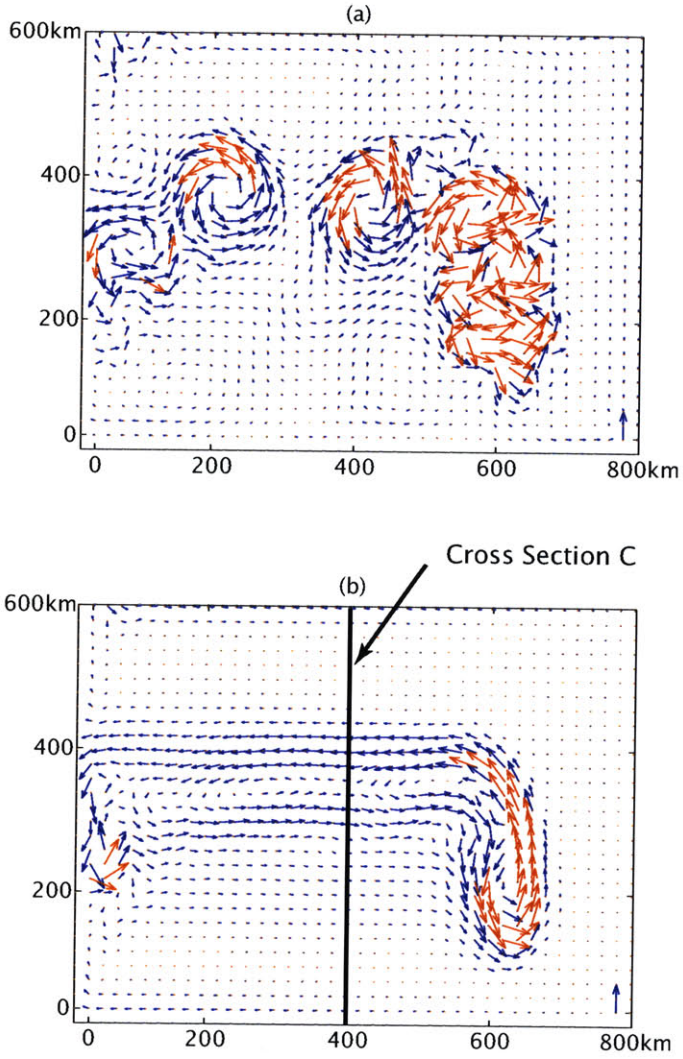

Figure 4-4: The Velocity field in layer 3 for the barotropic nonlinear case with a Gaussian bump (Case 3). (a) shows the instantaneous velocity field and (b) shows the mean velocity field. Velocity vectors larger than 0.01 m/s are truncated and are shown in red. For scaling, 0.01 m/s is shown in the down right corner. Figure (a) is the instantaneous velocity field after 50years of spinup. The formation of eddies north of the bump, propagation to the west, and dissipation at the western boundary can be seen from this figure. Figure (b) is the time mean velocity field. The mean flow shows the strong recirculation around the bump with two zonal jets. However, no particular mean structure can be seen in the region of these zonal jets in Figure (a) which indicates that the two mean zonal jets are the mean of eddies. The eastward zonal jet is broader than the northward zonal jet.

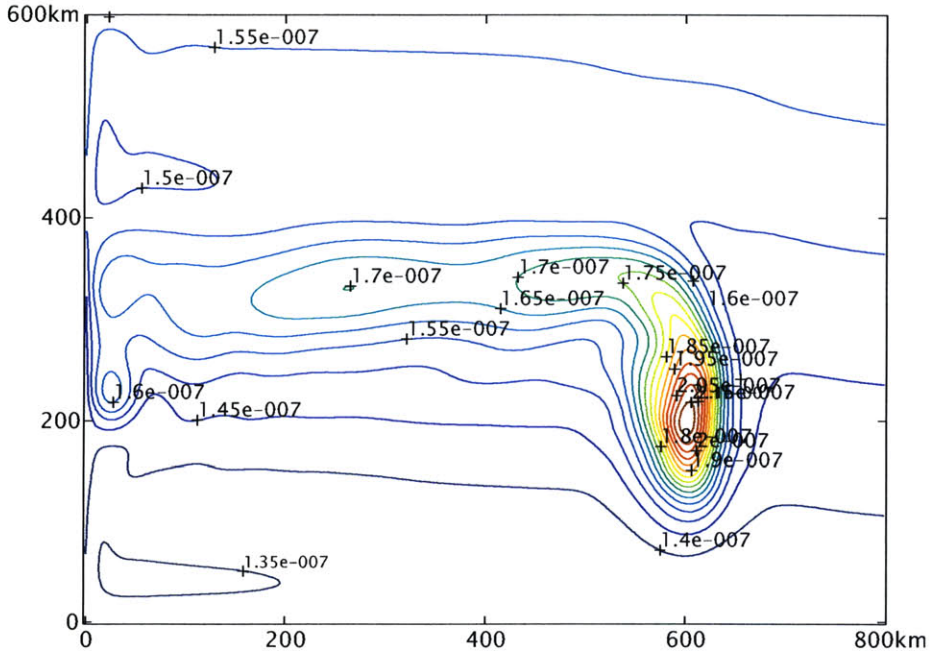

Figure 4-5: Mean PV field in layer 3 for the barotropic nonlinear case with a Gaussian bump (Case 3). The PV contours in the forcing region and the western boundary are more connected than it is for the background PV contours (Figure 4-1). This is because the eddies modifies the PV field which as a result, makes the flow cross the closed PV contour more easily than the linear case. The southern region of the forcing region shows a similar PV field with the background PV.

solution (0.005 m/s, 0.11 Sv), both the velocity and the transport were larger and the second westward jet observed in the south disappeared. The mean PV field is shown in Figure 4-5. Compared to the linear solution where the flow was influenced only by the background PV gradient, the flow in this nonlinear case can feel the change of PV that the flow has created itself. The nonlinearity allowed the formation of eddies which then could transport mass across the closed PV contour instead of using friction. Therefore, the flow has created a mean PV field in which the PV contours in the forcing region and the western boundary are more connected than the linear case. In contrast to the region north of the bump, the PV field south of the bump is similar to that in the linear case. The eddies seem to have modified the mean PV in the north of the bump but not much in the south.

The existence of eddies and the decrease in the recirculation strength can be explained by the existence of barotropic instability. Barotropic instability draws on the mean kinetic energy to weaken and smooth the flow. For a purely zonal flow, the necessary condition for this instability is that the meridional vorticity gradient change sign. As Figure 4-6 shows, the background vorticity gradient already satisfies this necessary condition (see Chapter 2 for details):

$$\beta + \frac{f}{H_o}\frac{\partial h_b}{\partial y} < 0 \tag{4.5}$$

Therefore whether the flow is weak or strong, the flow is likely to be unstable[2]. Eq 4.5 implies that the condition for barotropic instability can roughly be controlled by changing the background topography. For experiments where the maximum height of the bump (h_o) was small so that the topographic β^* is not large enough to satisfy Eq 4.5, the flow was stable. This condition for instability ($\beta - \beta^* < 0$) is also exactly the same condition for the existence of closed background PV contour region. The existence of closed background PV contour resulted in a strong recirculation in the linear case. However, the condition for barotropic instability shows that the extremely strong frictional recirculation will not establish when nonlinearity is included into the

[2]This assumption is true unless the flow has an extremely strong vorticity gradient that can change the background vorticity gradient.

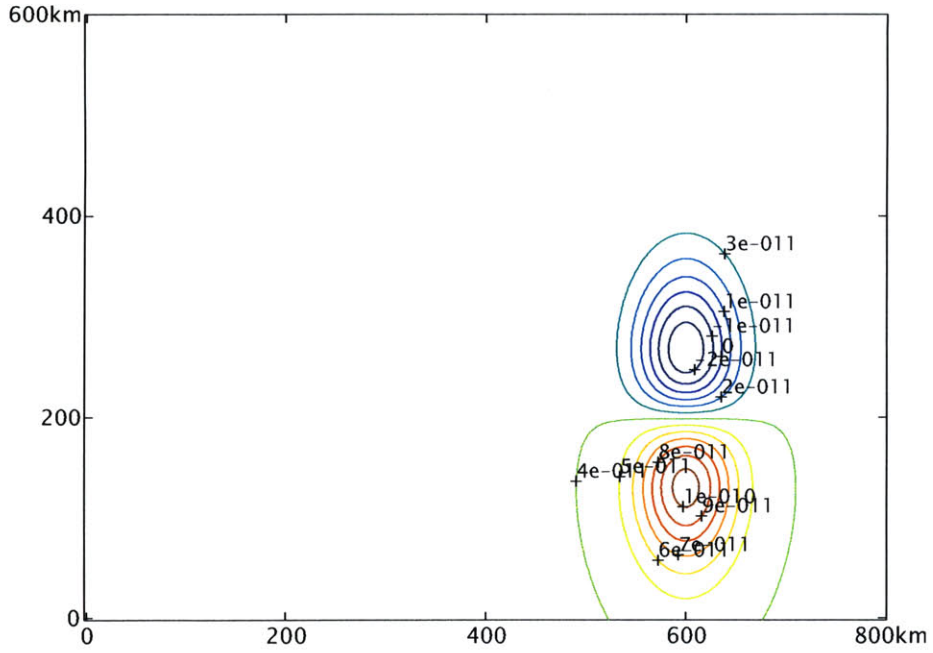

Figure 4-6: The meridional background vorticity gradient in layer 3 for a barotropic nonlinear case with a Gaussian bump (Case 3). If there were no Gaussian bump, the vorticity gradient is just the planetary vorticity gradient (which is constant for a β-plane) and this figure would have no contours. However the effective beta created by the the Gaussian bump introduces a change in the meridional vorticity gradient field. The gradient increased south of the bump but decreased north of the bump. The gradient also became negative north of the bump.

model.

The difference from the flat bottom case or a linear case with the Gaussian bump was the existence of eddies. One aspect of the role of these eddies can be seen from the layer thickness balance. Figure 4-7 shows the thickness balance along cross section C. Most of the forcing region shows a balance between the mean transport divergence and forcing but toward the northern part of the forcing region, the eddy transport divergence becomes more important in the balance. In fact, just outside the northern forcing region, there is a region where the balance is just between the mean and eddy transport divergence; this indicates that the mean flow is driven by eddies in this region. This region does match with where eddies were formed and from this plot, it shows that these eddies were transporting layer thickness into the forcing region from

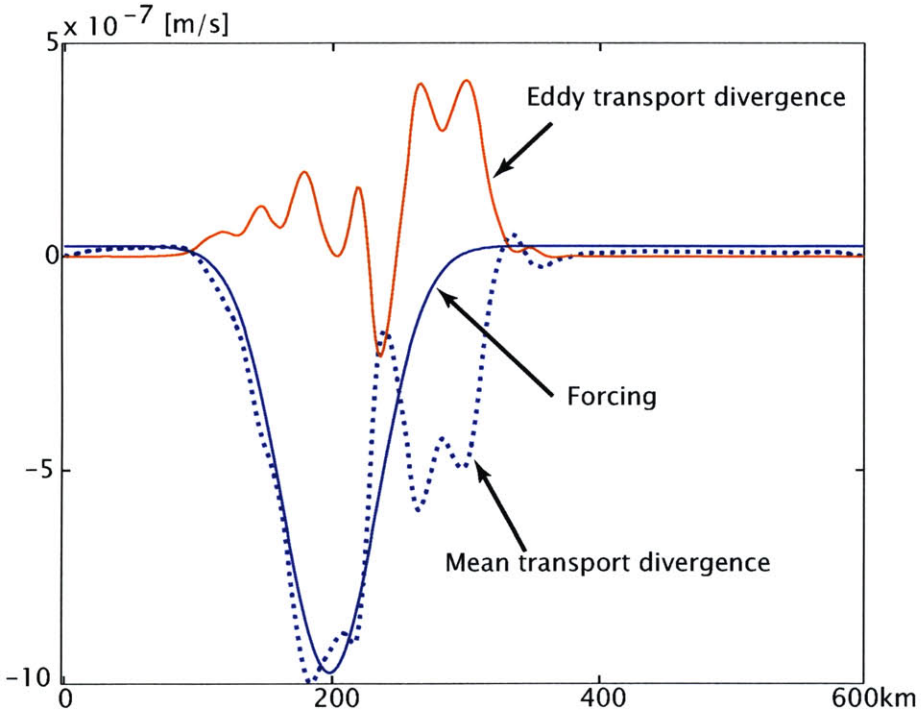

Figure 4-7: Layer thickness balance in layer 3 for a barotropic nonlinear case with a Gaussian bump (Case 3). Each of the term in the layer thickness equation is plotted along cross section A. (This cross section crosses the center of the forcing and the Gaussian bump.) North is to the right. Notice that the mean transport divergence matches with the forcing in the south of the forcing region. Eddy transport divergence becomes significant in size to the north and starts to balance the mean transport outside the forcing region. This is the area where the mean PV field (Figure 4-5) was modified the most.

the outside. This layer thickness transport by the eddies is one aspect of how the mean PV field shown in Figure 4-5 was created. The eddies formed in the north of the Gaussian bump where the flow is barotropically unstable, and then propagated to the western boundary. The eddies formed roughly every 10 years and after the eddies were out of the unstable region, the eddies propagated to the western boundary with a phase speed roughly 2×10^{-4} m/s and a wavelength 200 km. This agrees well with the Rossby wave dispersion relation for the long linear waves. The eddies formed north of the bump modified the mean PV field and propagated as long Rossby waves to the western boundary.

4.3 Baroclinic β-plume: Case 4

Baroclinicity was then included by using a nonlinear baroclinic model (Case 4). This case includes the effect of topography, baroclinicity and nonlinearity and is the case which created the result previously shown in Chapter 1 (Figure 1-4). Now, the complicated flow of Figure 1-4 can be better understood by using the understandings gained from previous cases.

The flow became statistically steady after 100 years of spin up (Figure 3-4). Instantaneous and time mean field of the velocity and the thickness deviation field in layer 3 are shown in Figure 4-8 and 4-9. Corresponding plots for layer 2 are shown in Figure 4-10 and 4-11.

The flow in layer 3 will be described first. The structure of the mean flow is similar to the previous barotropic experiment. The two zonal jets are shifted northward and a recirculation exists around the Gaussian bump. However, the maximum velocity and transport of the recirculation have decreased dramatically to 0.003 m/s and 0.07 Sv compared to the barotropic case (0.02 m/s and 0.34 Sv). The maximum velocity and transport of the zonal jet also decreased to 0.004 m/s and 0.03 Sv (compared to 0.01 m/s and 0.20 Sv).

The zonal transport along cross section C is shown in Figure 4-3. Like the flat bottom cases, the velocity and transport values showed a significant drop when baro-

clinicity was included. The values are now similar to that of Case 2 than Case 3 and the flow is also broad around the forcing region. This is because of baroclinic instability. The maximum velocity shear between the two layers in the forcing region was roughly 0.006 m/s which does satisfy the necessary condition for baroclinic instability (described in chapter 2, Eq 2.39): or,

$$|u_s| = 0.006m/s > u_c = 0.001m/s \tag{4.6}$$

However, the critical shear u_c that is used here was solved for a flow with a flat bottom. It does not include the effect of topographic variation which would likely to alter the critical value that is necessary for instability. The exact effect of topography variation needs more careful examination but model calculations with a variety of different parameter values indicate that the flat bottom criteria is a reliable (but rough) measure of the onset of baroclinic instability.

Barotropic instability also occurred in layer 3 because of the unstable background vorticity gradient (Figure 4-6):

$$\beta + \frac{f}{H_o}\frac{\partial h_b}{\partial y} < 0. \tag{4.7}$$

Eddies similar to the one mentioned in previous case 3 existed and can be seen as the relatively large eddies near the zonal jets in the snap shot of Figure 4-9. These eddies are large compared to the ones found near the forcing region which is another indication that the eddies are created by barotropic instability, not by baroclinic instability.

The flow in layer 2 had a maximum mean velocity and a transport of 0.004 m/s and 0.08 Sv in the forcing region. Both values became similar to the values in case 2 like layer 3. The mean velocity and transport values do not seem to have been affected by the existence of the Gaussian bump. However, the structure of the β-plume in layer 2 has changed dramatically by the Gaussian bump. The major difference from case 2 (Figure 3-5 or 3-6) is the existence of a second mean circulation north of the main β-plume. This circulation is due to the eddies created by the Gaussian bump

in layer 3 which would not have existed without the bump and nonlinearity. The southern shift of the main β plume is also an effect of the Gaussian bump. The strong recirculation around the topography in layer 3 changed the layer thickness in layer 2 so much that the mean PV field in layer 2 created a region of closed PV contour (Figure 4-12). Because this closed PV contour region had a minimum instead of a maximum like layer 3, the β plume shifted southward instead of northward.

The three cases with the Gaussian bump shown in this chapter can be interpreted as an example of how background PV influences the β-plume. The results show that the structure and the strength of the β-plume depend critically on the background PV distribution, especially for layer 3. Layer 2 was affected by the topography through the strong recirculation along the topography and the eddy activity in layer 3. Background PV can also be changed by other factors such as a mean zonal flow. The main difference between the effect of a mean zonal flow and the topography would be that a mean zonal flow will directly affect the circulation in both layers while topography can only affect layer 2 indirectly through the action of eddies or a strong recirculation around the topography in layer 3.

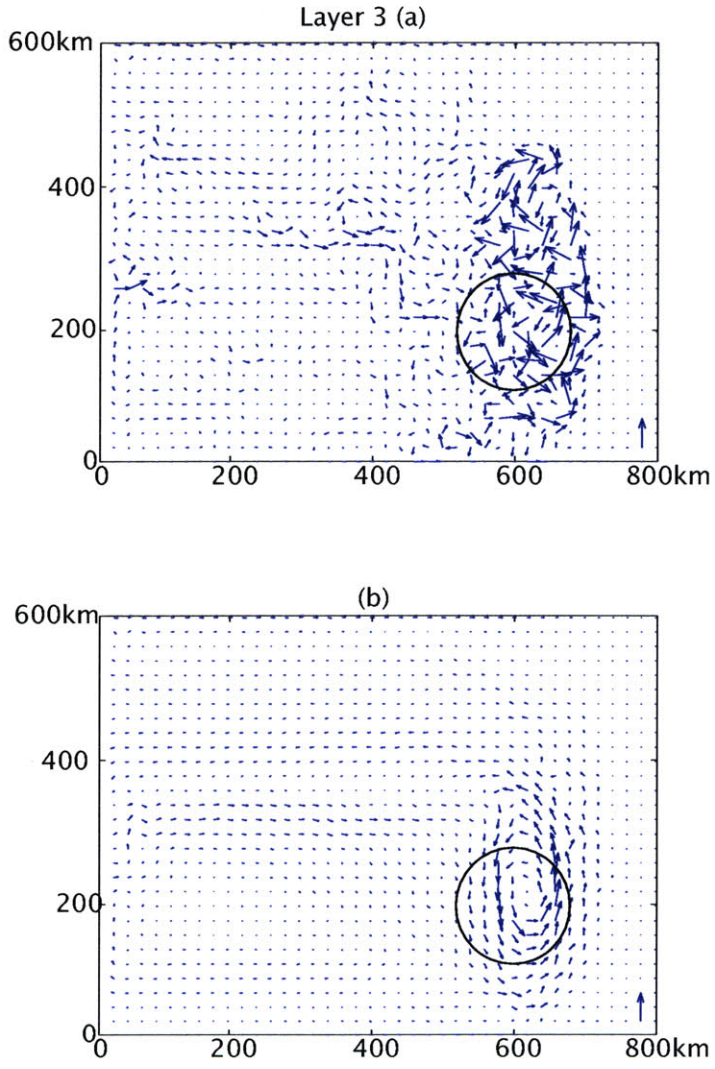

Figure 4-8: Velocity field in layer 3 for a baroclinic nonlinear case with a Gaussian bump (Case 4): (a) is the instantaneous velocity field after 100 years of spinup and (b) is the mean velocity field. Velocity vectors larger than 0.01 m/s are truncated and are shown in red. For scaling, 0.01 m/s is shown in the down right corner. The forcing region is indicated in a black circle. The instantaneous velocity field (a) shows active eddies around the forcing region. The mean velocity field (b) shows a structure similar to the barotropic case (case 3) but the size of the velocity is much less.

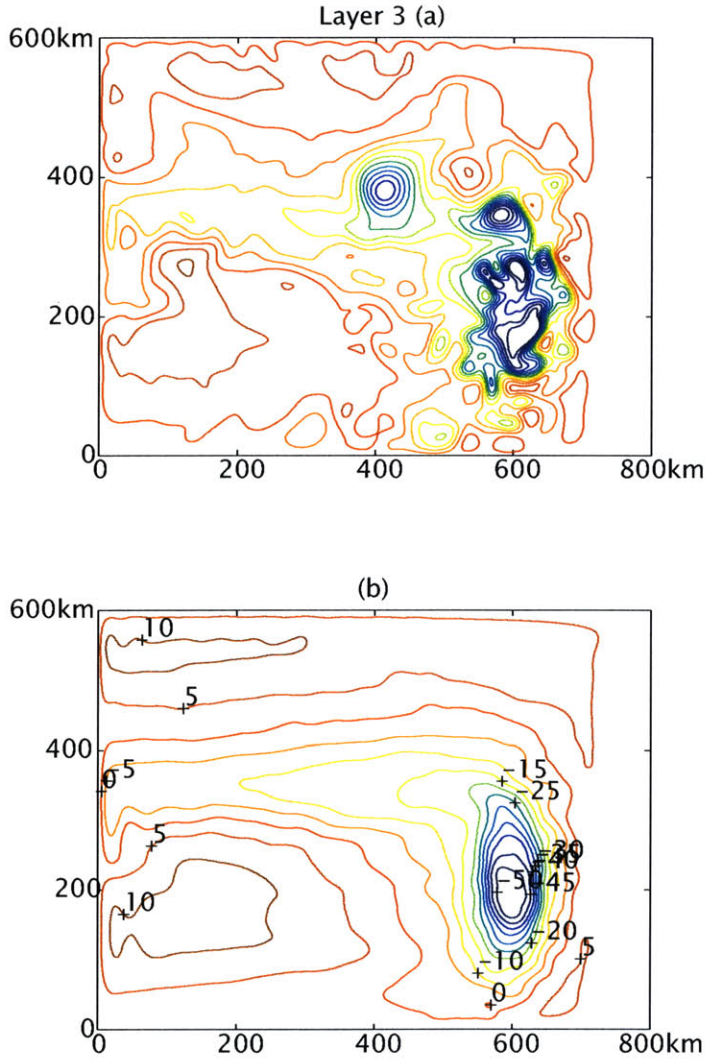

Figure 4-9: Pressure field in layer 3 for a baroclinic nonlinear case with a Gaussian bump (Case 4): (a) is the instantaneous pressure field after 100 years of spinup. and (b) is the mean pressure field. The contour values shown are $h_2' + 2h_3'$ with an interval of $50m$ for both plot. ($h_2' + 2h_3' = \rho_o g' P_3$) where $'$ is the fluctuation from the initial state). Like the velocity field, (a) shows active eddies near the forcing region. There is also a topographically induced eddies with a well defined structure where the zonal jets exist. These eddies are more clearly shown in this figure than in the previous figure of the velocity field. The mean field (b) shows a structure close to the barotropic case (Case 3) but the contours near the forcing region are more spread out.

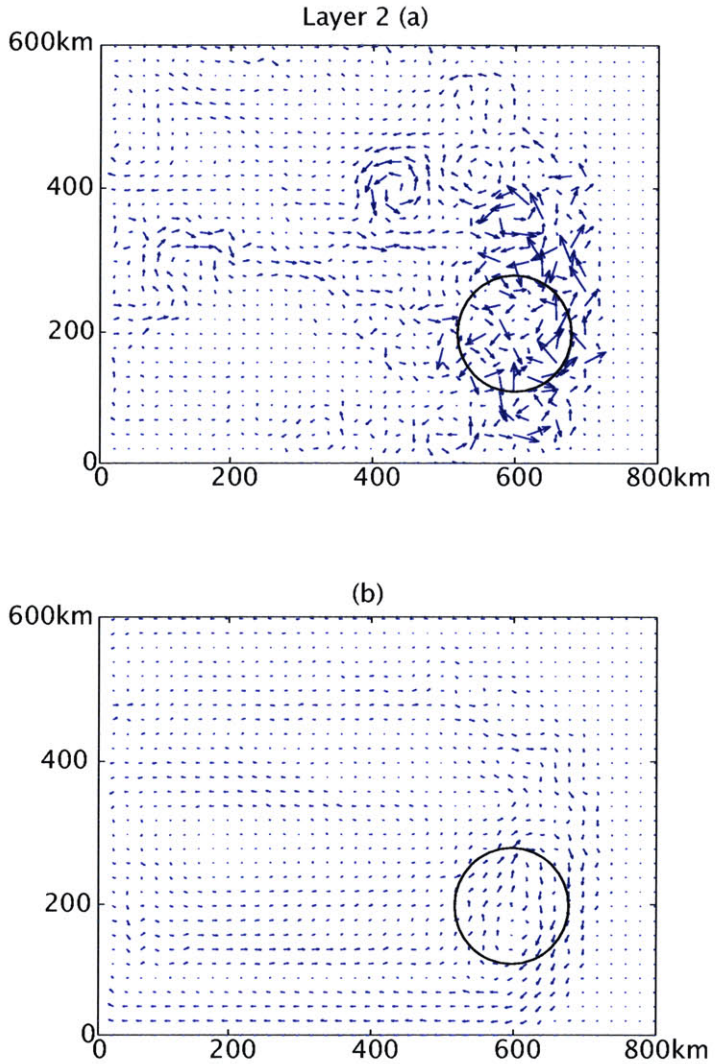

Figure 4-10: Velocity field in layer 2 for a baroclinic nonlinear case with a Gaussian bump (Case 4): (a) is the instantaneous velocity field after 100 years of spinup and (b) is the mean velocity field. Velocity vectors larger than 0.01 m/s are truncated and are shown in red. For scaling, 0.01 m/s is shown in the down right corner. The forcing region is indicated in a black circle. Like layer 3, the instantaneous velocity field (a) shows a very eddy dominated field around the forcing region. A well defined eddy can be seen in the middle of the basin. This is likely to be created by the topographically induced eddies in layer 3. The mean velocity field (b) shows a structure different from a baroclinic nonlinear flat bottom case (Case 2). The β-plume seems to have shifted southward but the whole circulation is weak and hard to see.

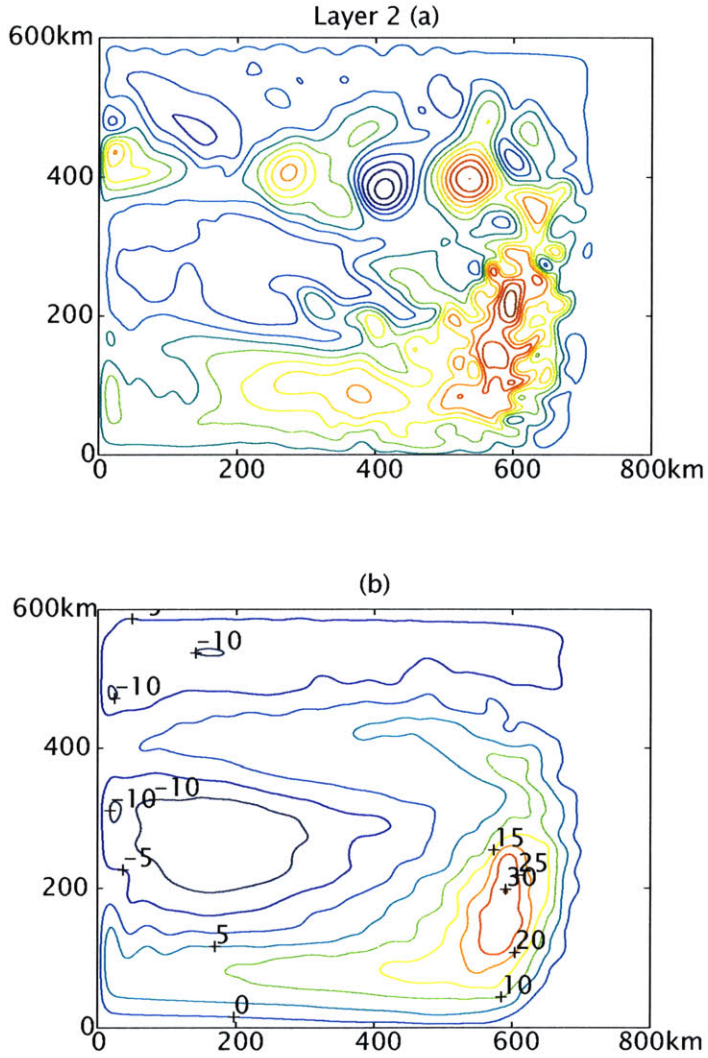

Figure 4-11: Pressure field in layer 3 for a baroclinic nonlinear case with a Gaussian bump (Case 4): (a) is the instantaneous pressure field after 100 years of spinup. and (b) is the mean pressure field. The contour values shown are $h_2' + 2h_3'$ with an interval of $50m$ for both plot. ($h_2' + 2h_3' = \rho_o g' P_3$) where $'$ is the fluctuation from the initial state). Like the velocity plots, the instantaneous field (a) shows active eddies near the forcing region. The eddies in the middle of the basin are created by the topographically induced eddies in layer 3 and is more clear here than in the previous figure (Figure 4-10). The mean field (b) shows the southern shift of the β plume clearly. There is also a second circulation in the north. This circulation is created by the topographically induced eddies in layer 3 that propagated to the western boundary along this latitude.

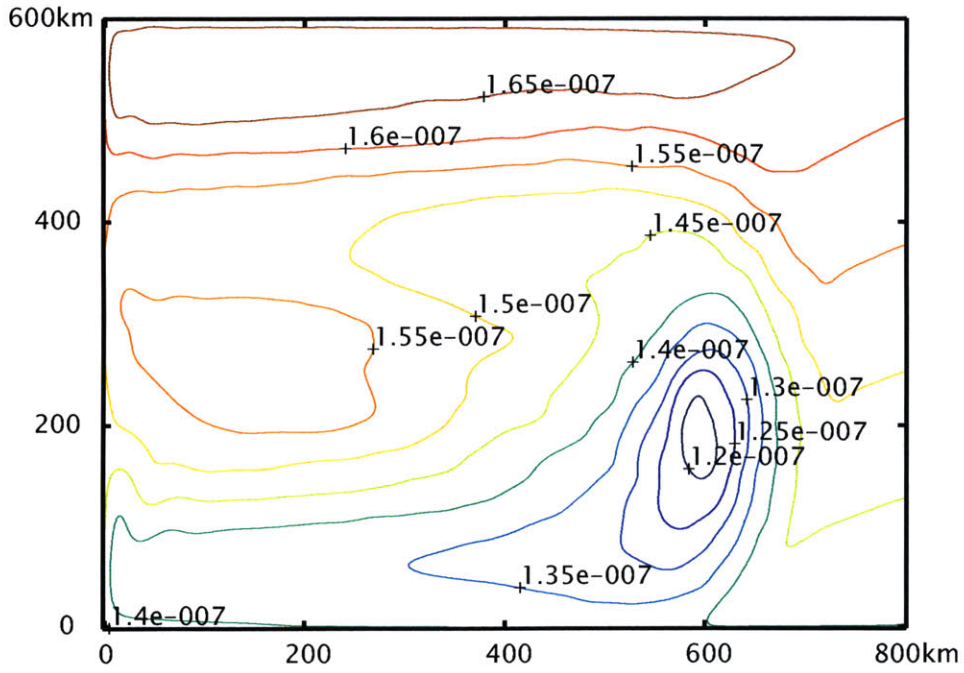

Figure 4-12: Time mean PV field for layer 2 in a baroclinic nonlinear case with a Gaussian bump (Case 4). Although the PV in this layer is not directly affected by the bottom topography, the strong recirculation in layer 3 has created a region of closed PV contour near the forcing region. This closed PV contour region has a lower PV than its surroundings which therefore results in a southern shift in the main structure of the β-plume.

Chapter 5

Summary and Conclusion

The concept of β plumes is inspiring for two things. First, for the establishment of strong zonal jets and second, for driving a large horizontal circulation by a small region or strength of the mass source/sink. However, these results are based on a linear theory. A numerical calculation showed that the β plume in the deep ocean was remarkably different and complicated than the linear solution when nonlinear dynamics and instabilites were permitted (Figure 1-4). In order to understand the dynamics of how this complicated flow field was achieved, the problem was separately examined on the effect of baroclinicity and topographic variation.

5.1 Summary

The effect of baroclinicity was examined in two steps. A nonlinear barotropic β plume was compared to the linear solution to examine the effect of nonlinearity. Then a nonlinear baroclinic β plume was compared to the nonlinear barotropic β plume to examine the effect of baroclinicity. The effect of topographic variation was examined next using three illustrative cases. Using a Gaussian bump for topographic variation, a linear barotropic β plume was compared to that of a flat bottom first. Then nonlinearity was added into the barotropic model and finally baroclinicity was added to examine the case with both baroclinicity and topographic variation.

The model used in this study had a motionless layer above and a moving layer(s)

below [Figure 2-1] to represent the deep ocean flow. One-and-a-half layer model was used to study the barotropic response of a β-plume and two-and-a-half layer model was used to study the baroclinic response of a β-plume. The only difference between the two models is whether the intermediate layer of the two-and-a-half layer model is moving or not. A cross isopycnal velocity(w^*) is prescribed between the bottom layer and the intermediate layer. An intense cross isopycnal velocity from the bottom layer to the intermediate layer exists in a localized region in the interior and a weak flow back from the intermediate layer to the bottom layer exists uniformly across the basin to conserve the mass in each layer. This prescribed cross isopycnal velocity is the forcing in this model. The parameters g' and w^* were chosen from observations of a hydrothermal plume in the Juan de Fuca Ridge in *Baker (1987)*.

First two cases were on β-plumes with a flat bottom.

The nonlinear barotropic β-plume (Case 1) had a structure similar to the linear solution. The magnitude of the transport was also similar to the linear solution. The major difference was the existence of waviness in the eastward zonal jet (Figure 3-1) which the feature existed only when the inertial boundary layer width was larger than the Munk boundary layer width. This was a standing Rossby wave which had a phase speed exactly opposite to the mean flow and matched with the theoretical wavelength and dissipation length scale ($\lambda = \sqrt{u_{jet}/\beta}$ and $l = u_{jet}^2/\beta A_H$ respectively) estimated from an assumption that the velocity of the zonal jet (u_{jet}) was zonally uniform. The eastward zonal jet was also barotropically unstable close to the western boundary. The necessary condition for barotropic instability was met in this area and so the waviness mentioned previously occasionally broke due to this instability. The vorticity balance in the intense cross isopycnal transport region (referred to as the forcing region) was still between the two linear terms, i.e. planetary vorticity advection and the stretching term. This held true even in the case with the standing Rossby wave or barotropic instability[1]

The baroclinic β-plume with a flat bottom (Case 2) did not reach a steady state

[1]The linear vorticity balance will be valid as long as the dissipation length scale of the standing Rossby wave is less than the distance from the forcing region to the western boundary.

but reached a statistically steady state. In a snapshot of this statistically steady state, the structure of the flow was hard to discern and the velocity field was dominated by eddies. However, the time mean flow of this steady state did show a β-plume with a structure similar to the barotropic case although its maximum velocity and transport of the zonal jets were smaller and broader. Baroclinic instability was responsible for this decrease in the magnitude of the zonal jets. The mean flow satisfied the necessary condition for baroclinic instability. Although this necessary condition makes an assumption of purely zonal flows which is admittedly crude for β plumes, many numerical calculation showed that it is still an adequate indicator of baroclinic instability. Baroclinic instability converts the potential energy of the mean flow to the eddies and as a result, it prevents the flow from creating a large shear between the layers. The eddies created by baroclinic instability also played a crucial role in balancing the forcing. In layer 3, the thickness balance in the forcing region showed the eddies advecting layer thickness from outside the forcing region that was balancing the mass lost in the forcing region, not the mean flow. This advection of layer thickness by eddies happened mostly around the eastern half of the forcing region. The PV balance in the forcing region also showed the eddy PV flux balancing the PV forcing. Eddies redistributed layer thickness and PV with the region outside the forcing region and as a result drove a mean flow there. This was why the mean flow was broader than the barotropic case. The eddies in this baroclinic case made the β-plume weaker and broader; in this sense, the eddies had a diffusive effect on the flow.

The next three cases were on β-plumes with topographic variation. A Gaussian bump was used for bottom topography which changed the PV background and created a region of closed PV contours. This changed the structure of the β-plume from a flat bottom case dramatically.

The linear solution had an extremely strong cyclonic recirculation in the closed PV contour region. This was because forcing existed within the closed PV contour region which friction became essential to transporting mass across the closed PV contour in order to create an ageostrophic component of the flow. The transport of the zonal

jets were less than the linear solution with a flat bottom.

The nonlinear barotropic flow (Case 3) started to have eddies developing at the north of the bump. In a nonlinear system, eddies can create a net transport across the closed PV contour. This contrasts to the linear case in which friction was the only mechanism that could transport across closed PV contours. As a result, the strong recirculation around the bump became smaller than that of linear case and the magnitude of the zonal jets increased instead. the latitude of the zonal jets have shifted southward due the modification of the mean PV gradient field by the eddies. The eddies that developed at the north of the bump eventually traveled to the western boundary and dissipated.

The final case included both baroclinicity and a Gaussian bump (Case 4). The flow exhibited both of the features that were observed in the baroclinic flat bottom case (Case 2) and the barotropic topography case (Case 3). Layer 3 had a structure similar to case 3 showing the effect of the background PV by the Gaussian bump to the flow. However, the strength of the flow was closer to case 2 showing that the existence of baroclinic instability determined the strength of the flow. The strength of the flow in layer 2 was also close to that found in case 2 likely to be for the same reason. There were two big differences compared to cases 2 and 3. First, a new circulation in layer 2 existed north of the usual β-plume. This was due to the topographically induced eddy activity in layer 3. Second, a closed PV contour region was also created in layer 2 by the strong recirculation around the bump in layer 3. This resulted in the southern shift of the β plume in layer 3. The flow in layer 2 was shown to be affected by the existence of topographic variation.

5.2 Concluding Remarks

β-plume dynamics in the deep ocean was found to be remarkably different from what would be expected from a linear solution when nonlinear dynamics and instabilities were permitted. Barotropic and baroclinic instability occurred and created eddies which played an important role in balancing layer thickness and PV. The eddies cre-

ated by baroclinic instability had diffusive character whereas the eddies created by topographically induced barotropic instability had more of an advective character. The topographically induced eddies also reduced the strength of the strong recirculation over the topography and drove a mean circulation in the layer that was not directly affected by the topography.

Since the large scale flow is thought to be weak in the deep ocean, one would imagine the deep ocean to be governed more on linear theory. However, deep ocean is weakly stratified and so the reduced gravity g' is very small. It requires a very steep isopycnal slope to drive a horizontal flow and thus the necessary condition for baroclinic instability can be easily satisfied. Baroclinic instability can occur even for a weak β-plume with velocity in order of 0.01 m/s. Therefore, for a localized forcing such as hydrothermal plumes, the eddies play a crucial role in its β-plume dynamics. Also because the deformation radius is of the order of few kilometers in the deep ocean and is much smaller than the inertial wave length ($\sqrt{u/\beta}$), baroclinic instability is likely to be an important process than barotropic instability.

How would β-plumes be observed in the ocean? It definitely will be difficult to find and observe the mean flow with a weak mean flow of order 0.01 m/s. Eddies of equal or larger magnitude will dominate and make it harder to see any structure unless a very long time mean is taken. This is because evolution of a flow in the ocean is very slow and one can not see a mean structure unless the mean is taken over few tens of years. The background topography or flow may very well change the structure and further complicate observation of the β-plume as the cases with the Gaussian bump topography suggests. More careful examination of how β-plumes are affected by the background needs to be done if it were to be compared directly to observations. Distribution of tracers could help us in determining where and how strong the β-plume is. Although tracer distribution does not follow exactly with the flow (*Speer 1988*) but nonetheless it could still reveal some aspects of β-plume dynamics in the deep ocean.

The idea of β-plumes have been applied to overflows where the entrainment of ambient ocean water into overflows happen locally (see Chapter 1). For the ambient

ocean, this entrainment is a local mass sink which is similar to the situation of layer 3 in this study (where mass is lost to layer 2). However, adaption of the β-plume dynamics considered in this study to β plumes by overflows requires some crucial adjustments to the model parameters: the reduced gravity and the forcing strength. For overflows, the reduced gravity is larger and cross isopycnal transport is more intense (*Baringer and Price 1997*). The structure of the long time mean might look similar but unlike the deep ocean β plumes, barotropic instability would probably be more prevalent than baroclinic instability because the inertial wave length would be comparable to the deformation radius. This seems to be exactly the case for the numerical model results in *Özgökmen (2000)*. Since barotropic instability requires large horizontal velocity shear, it is likely to have a very strong flow which could make β-plume more easier to observe than the β-plume in the deep ocean.

Future work will include a more careful examination of the necessary condition for instability because the instability developed not at the zonal jets but where the flow was more meridional in the forcing region. The influence of bottom topography on baroclinic instability also needs to be considered because the difference in layer thickness changes the condition for instability which can either destabilize or stabilize the flow depending on the sign of the effective β created by the topography. The presence of mean background flow can also change the condition for instability because it introduces a new background PV gradient field equally to different layers. Many works examining the effect of the background flow on β-plumes [e.g. *Speer 1987*] are based on linear β-plume dynamics or focused on single plume events, but this study indicates that topography and eddies are also important for the large scale plumes. Parameterization of eddies shown in the model would also be a very interesting problem to work on. Although this is by all means a very difficult problem, by examining the role of eddies in a model that is simple enough to understand but complex enough to exhibit instability, we may be able to gain further insight into the role of eddies and its parameterization in the deep ocean.

Bibliography

Baringer, M.O. and J.F. Price (1997). Mixing and spreading of the mediterranean outflow. *J. Phys. Oceanogr.*, 27:1654–1677.

Cessi, P., R.G. Condi, and W.R. Young (1990). Dissipative dynamics of western boundary currents. *J. Mar. Res*, 48:677–700.

D'Asaro, E., S. Walker, and E. Walker (1994). Structure of two hydrothermal megaplumes. *J. Geophys. Res.*, 99:20361–20373.

Özgökmen, T.M. and F. Crisciani (2001). On the dynamics of β plumes. *J. Phys. Oceanogr.*, 31:3569–3580.

Özgökmen, T.M., E.P.Chassignet, and C.G.H. Rooth (2001). On the connection between the mediterranean outflow and the azores current. *J. Phys. Oceanogr.*, 31:461–480.

Flierl, G.R. (1988). On the instability of geostrophic vortices. *J. Fluid. Mech.*, 197:349–388.

Hautala, S.L. and S.C Riser (1993a). A nonconservative β-spiral determination of the deep circulation in the eastern south pacific. *J. Phys. Oceanogr.*, 23:1975–2000.

Hautala, S.L. and S.C. Riser (1993b). A simple model of abyssal circulation, including effects of wind, buoyancy and topography. *J. Phys. Oceanogr.*, 23:1975–2000.

Helfrich, K.R. and T. Battisti (1991). Experiments on barolinic vortex shedding from hydrothermal plumes. *J. Geophys. Res.*, 96:12511–12518.

Helfrich, K.R., T.M. Joyce, G.A. Cannon, S.A. Harrington, and D.J. Pashinski (1998). Mean hydrographic and velocity sections near pipe organ vent at juan de fuca ridge. *Geophys. Res. Letters*, 25(10):1737–1740.

Helfrich, K.R. and U. Send (1988). Finite-amplitude evolution of two-layer geostrophic vortices. *J. Fluid Mech.*, 197:331–348.

Helfrich, K.R. and K.G. Speer (1995). Oceanic hydrothermal circulation:mesoscale and basin-scale flow. agu monograph 91, seafloor hydrothermal systems physical, chemical, biological, and geological interactions.

Hogg, N.G. and H.M Stommel (1985). The heton, and elementary interaction between discrete baroclinic geostrophic vortices, and its implications concerning eddy heat flow. *Proc. R. Soc. Lond.*, 397:1–20.

Holland, W.R. and L.B. Lin (1975). On the generation of mesoscale eddies and their contribution to the oceanic general circulation. i. a preliminary numerical experiment. *J. Phys. Oceanography*, pages 642–657.

Jia, Y. (2000). The formation of an azores current due to mediterranean overflow in a modeling study of the north atlantic. *J. Phys. Oceanogr.*, 30:2342–2358.

Joyce, T.M., G.A. Cannon, D. Pashinski, K.R. Helfrich, and S.A. Harrington (1998). Vertical and temporal vorticity observations at juan de fuca ridge: hydrothermal signatures. *Geophys. Res. Letters*, 25(10):1741–1744.

Joyce, T.M. and K.G. Speer (1987). Modeling the large-scale influence of geothermal sources on abyssal flow. *J. Geophys. Res.*, 92:2843–2850.

Kawase, M. (1987). Establishment of deep ocean circulation driven by deep water production. *J. Phys. Oceanogr.*, 17:2294–2317.

Kawase, M. and D.N. Straub (1991). Spinup of source-driven circulation in an abyssal basin in the presence of bottom topography. *J. Phys. Oceanogr.*, 21:1501–1514.

Lupton, J.E. and H. Craig (1985). A major helium-3 source at $15^o s$ on the east pacific rise. *Science*, pages 13–18.

Moore, D.W (1963). Rossby waves in ocean circulation. *Deep-Sea Res*, 10:735–747.

Pedlosky, J. (1987). *Geophysical Fluid Dynamics*, volume 710pp. Springer-Verlag, Berlin.

Pedlosky, J. (1996). *Ocean Circulation Theory*, volume 543pp. Springer-Verlag, Berlin.

Spall, M. (2001). Large-scale circulations forced by localized mixing over a sloping bottom. *J. Phys. Oceanogr.*, 31:2369–2384.

Spall, M.A. (2000). Buoyancy-forced circulations around islands and ridges. *J. Mar. Res.*, 58:957–982.

Speer, K.G. (1988). *The influence of geothermal sources on deep temperature, salinity and flow fields.* Ph.D. thesis, MIT-WHOI Joint Program in Oceanography.

Speer, K.G. (1989). A forced baroclinic vortex around a hydrothermla plume. *Geophys. Res. Lett.*, 16(5):461–464.

Speer, K.G and J. Marshall (1995). The growth of convective plumes at seafloor hot springs. *J. Mar. Res.*, 53:1025–1057.

Stommel, H. and A.B. Arons (1960a). On the abyssal circulation of the world ocean- i. stationary planetary flow patterns on a sphere. *Deep-Sea Res.*, 6:140–154.

Stommel, H. and A.B. Arons (1960b). On the abyssal circulation of the world ocean -ii. an idealized model of the circulation pattern and amplitude in oceanic basins. *Deep-Sea Res.*, 6:217–233.

Stommel, H.M. (1982). Is the south pacific helium-3 plume dynamically active? *Earth Planet. Sci. Lett.*, 61:63–67.

Straub, D.N. and P.B. Rhines (1990). Effects of large-scale topography on abyssal circulation. *J. Mar. Res.*, 48:223–253.

Yang, J. and J.F. Price (2000). Water-mass formation and potential vorticity balance in an abyssal ocean circulation. *J. Mar. Res.*, 58:789–808.